Axonal ER Ca^{2+} Release Enhances Miniature, but Reduces Activity-Dependent Glutamate Release in a Huntington Disease Model

James P. Mackay[1], Amy I. Smith-Dijak[1,2], Ellen T. Koch[1,2], Peng Zhang[1], Evan Fung, Wissam B. Nassrallah[1,3], Caodu Buren[1,2], Mandi Schmidt[2,4], Michael R. Hayden[4] and *Lynn A. Raymond[1]

[1] Department of Psychiatry, Djavad Mowafaghian Centre for Brain Health,

[2] Graduate Program in Neuroscience

[3]MD/PhD Program

[4] Centre for Molecular Medicine and Therapeutics, BC Children's Hospital Research Institute

University of British Columbia, Vancouver, British Columbia, Canada

*Correspondence addressed to:

Lynn A. Raymond, MD, PhD

Department of Psychiatry and Djavad Mowafaghian Centre for Brain Health

University of British Columbia

4834-2255 Wesbrook Mall

Vancouver, BC Canada V6T 1Z3

Lynn.raymond@ubc.ca

Abstract

Action potential-independent (miniature) neurotransmission occurs at all chemical synapses, but remains poorly understood, particularly in pathological contexts. Spontaneous release of Ca^{2+} from the axonal endoplasmic reticulum (ER) is thought to facilitated miniature neurotransmission, and aberrant ER Ca^{2+} handling is notably implicated in the progression of Huntington's disease (HD) and other neurodegenerative diseases. Here, we report elevated glutamate-mediated miniature synaptic event frequencies in YAC128 (HD-model) cortical neurons, which pharmacological experiments suggest is mediated by enhanced spontaneous ER Ca^{2+} release. Calcium imaging using an axon-localized sensor revealed slow action potential (AP)-independent axonal Ca^{2+} waves, which were more common in YAC128 cortical neurons. Conversely, spontaneous axonal ER Ca^{2+} release was associated with reduced AP-dependent axonal Ca^{2+} events and consequent glutamate release. Together, our results suggest spontaneous release of axonal ER Ca^{2+} stores oppositely regulates activity-dependent and -independent neurotransmitter release in HD, with potential implications for the fidelity and plasticity of cortical excitatory signaling.

Introduction

Huntington's disease (HD) is a fatal, autosomal dominantly-inherited neurodegenerative disorder caused by a polyglutamine-encoding CAG repeat-expansion (>35 repeats) in exon-1 of the huntingtin gene ("A novel gene containing a trinucleotide repeat that is expanded and unstable on Huntington's disease chromosomes. The Huntington's Disease Collaborative Research Group.,"

49 1993). Disease onset is typically in middle age, characterized by progressively disordered
50 movement and declining cognition (Bachoud-Lévi et al., 2019). Although the mutant huntingtin
51 protein (mHTT) is widely expressed, GABAergic spiny projection neurons (SPN)s of the striatum
52 and pyramidal neurons of the cerebral cortex show the most severe degeneration in HD
53 (Graveland, Williams, & DiFiglia, 1985; Vonsattel et al., 1985). Cortical glutamatergic afferents
54 extensively innervate striatal SPNs and dysfunction at these synapses is thought to precede overt
55 neuron loss in HD (Raymond et al., 2011).
56
57 Glutamate-mediated toxicity was initially proposed to contribute to pathogenesis in HD based on
58 studies showing that striatal injections of glutamate receptor agonists largely recapitulate HD
59 pathology in animals (Beal et al., 1986; Hantraye, Riche, Maziere, & Isacson, 1990). More
60 recently, studies in SPNs from transgenic and knock-in mouse models of HD demonstrate
61 enhanced extrasynaptic N-Methyl-D-Aspartate receptor (NMDAR) surface expression and
62 function that may explain, in part, increased susceptibility to excitotoxic challenges (Botelho et
63 al., 2014; Fan, Fernandes, Zhang, Hayden, & Raymond, 2007; Kovalenko et al., 2018; Milnerwood
64 et al., 2010; Plotkin et al., 2014; Zeron et al., 2002). Cell stress/death signaling mediated by
65 elevated levels of extrasynaptic NMDARs in HD SPNs may be further exacerbated by reduced
66 glutamate transporter function (Miller et al., 2008), although recent studies show glutamate
67 clearance after synaptic release is normal or accelerated in striatal and cortical brain slice (Parsons
68 et al., 2016). Additionally, some studies show synaptic glutamate release from cortical afferents is
69 altered in HD mouse models, possibly contributing to excitotoxicity and synaptic dysfunction
70 (Cepeda et al., 2003; Joshi et al., 2009; Raymond et al., 2011). However, the direction of this effect

71 appears to be model and disease-stage dependent; relative to wildtype (WT), glutamate release is
72 typically enhanced early, but reduced with disease progression in HD mice (Joshi et al., 2009).
73
74 Mutant HTT (mHTT) directly interacts with endoplasmic reticulum (ER) type-1 inositol (1,4,5)-
75 triphosphate receptors (IP3Rs) sensitizing their Ca^{2+} release in response to IP3 (Tang et al., 2003);
76 blocking this interaction normalizes IP3-induced ER Ca^{2+} release *in vitro* and improves behavioral
77 outcomes in HD-model mice (Tang, Guo, Wang, Chen, & Bezprozvanny, 2009). Furthermore,
78 evidence suggests Ryanodine receptors, which are ER-localized Ca^{2+} channels that mediate Ca^{2+}-
79 induced Ca^{2+} release, are constitutively leaky in HD mouse models (Suzuki, Nagai, Wada, &
80 Koike, 2012). Although these studies focused on the soma and dendrites of SPNs at the
81 postsynaptic side of cortical-striatal synapses, ER is found in all neuronal compartments, including
82 presynaptic terminals, where its Ca^{2+} stores, when released, modulate neurotransmission
83 (Emptage, Reid, & Fine, 2001; Llano et al., 2000). However, it is unknown whether presynaptic
84 ER Ca^{2+} handling is also dysfunctional in HD and if such a process contributes to altered glutamate
85 release from cortical synaptic terminals.
86
87 Here, we have investigated whether glutamate release is altered, and if ER Ca^{2+} dysregulation
88 contributes to aberrant function, in presynaptic terminals of cortical pyramidal neurons from
89 premanifest HD-model mice expressing full-length mHTT with 128 CAG-repeats in a yeast
90 artificial chromosome (YAC128). Our results from neuronal cultures and acute cortical-striatal
91 brain slices demonstrate a shift in balance favoring increased action potential (AP)-independent
92 (miniature) vs. AP-dependent glutamate release, and that altered ER Ca^{2+} release contributes to
93 this change. This may have important previously unidentified disease implications, given the

94 distinct physiologically relevant signaling potentially mediated by miniature neurotransmission
95 (Fishbein & Segal, 2007; Kavalali, 2015). Ultimately our data contribute to growing evidence for
96 cortex and striatal synaptic dysfunction in HD, and support a key role for ER Ca^{2+} dysregulation
97 in this pathophysiology.
98
99 **Results**
100
101 **Mini EPSC frequencies are elevated in YAC128 cortical cultures at early time points**
102
103 Our group previously recorded miniature excitatory post synaptic currents (mEPSCs) from striatal
104 spiny projection neurons (SPNs) co-cultured with cortical neurons from prenatal WT or yeast
105 artificial chromosome (YAC128) mice. YAC128 SPNs showed elevated mEPSC frequencies,
106 compared to WT, at day in vitro (DIV) 14 – a time point when SPN dendritic arborization patterns
107 and spine numbers were similar between genotypes (Buren, Parsons, Smith-Dijak, & Raymond,
108 2016). At DIV21, YAC128 SPNs showed a significant reduction in total dendritic length, and
109 therefore reduced total excitatory synapse numbers, compared to WT. Despite this, mEPSC
110 frequencies onto WT and YAC128 SPNs were comparable at DIV21.
111
112 The above results suggested a higher rate of action potential-independent glutamate release from
113 YAC128 presynaptic cortical pyramidal neuron (CPN) terminals onto individual SPN synapses.
114 Here, we capitalize on a relatively simpler culture preparation containing only cortex-derived
115 neurons and YAC128 mouse-derived brain slices to mechanistically dissect how mutant huntingtin

116 protein expression affects action potential-independent and -dependent glutamate release from
117 CPN terminals.
118
119 To establish whether miniature glutamate release is enhanced at YAC128 CPN terminals targeting
120 other CPNs, we first established WT and YAC128 CPN mEPSC parameters in cortical cultures at
121 various DIV ages (7, 14, 18 and 21). In general, both genotypes showed increased mEPSC
122 frequencies with culture time. However, YAC128 CPN mEPSC frequencies were consistently
123 higher than age-matched WT controls after DIV7 and up until DIV21, at which point mEPSC
124 frequencies became comparable between genotypes **(Figure 1),** as was also the case in the co-
125 culture model (Buren et al., 2016). The greatest genotype mEPSC frequency difference occurred
126 at DIV14, when mean YAC128 CPN frequencies were more than double that of WT: 10.83 ± 1.80
127 Hz vs 4.52 ± 0.60 Hz, respectively **(Figure 1D, E)**. YAC128 mEPSC frequencies remained
128 significantly higher than WT at DIV18: 14.07 ± 1.54 Hz vs 9.92 ± 1.54 Hz, respectively **(Figure**
129 **1G, H)**. Age matched YAC128 and WT CPNs showed similar mEPSC amplitudes across all DIV
130 time points examined **(Figure 1 C, F, I and L)**. We chose to perform subsequent experiments
131 probing the mechanistic details underlying increased cortical mini glutamate release in DIV18
132 cortical monocultures, since this was the most mature culture stage at which mEPSC frequencies
133 were elevated in YAC128 CPNs.
134
135
136
137

138 **Synapse numbers and dendritic complexity are similar in WT and YAC128 cortical**
139 **pyramidal neurons at DIV 18**
140
141 The higher mEPSC frequencies seen in DIV18 YAC128 CPNs suggest an increased presynaptic
142 glutamate release probability. However, relative differences in synapse numbers could also
143 account for this finding. To estimate numbers of synapses, we first expressed cytosolic GFP in a
144 small proportion of neurons in WT and YAC128 cortical cultures and imaged full CPN dendritic
145 arbors at DIV18. Sholl analysis revealed similar arborization patterns and total dendritic length in
146 WT and YAC128 CPNs **(Supplemental Figure 1A, C)**. In separate cultures, we expressed an
147 internal GFP-tagged anti-PSD95 antibody (Gross et al., 2013) in a subset of neurons and immuno-
148 stained for VGlut1, to identify glutamatergic terminals, and the GluA2 AMPA receptor subunit,
149 to identify functional synapses. Functional synapse numbers, defined as GFP-labeled PSD95
150 puncta colocalized with VGlut1 and GluA2 immunofluorescent-labeled puncta, were not
151 significantly different between DIV18 WT and YAC128 CPNs, although there was a trend towards
152 lower synapse density in YAC128 CPNs **(Supplemental Figure 1E, F)**. Together with the above
153 data showing increased mEPSC frequency in YAC128 CPNs at DIV18 **(Figure 1)**, these results
154 point to an increase in miniature vesicular glutamate release from cortical terminals in YAC128
155 cultures.
156
157
158
159

160 **Releasing ER calcium with low dose ryanodine or caffeine increases the miniature EPSC**
161 **frequency in WT, but not YAC128 cultures**
162
163 Studies using mouse models suggest Ca^{2+} release from ER stores is aberrant in HD due to increased
164 IP3 and ryanodine receptor activity (Suzuki et al., 2012; Tang et al., 2003). Although effects of
165 mHTT on the presynaptic ER have not been specifically studied, we hypothesized a presynaptic
166 ER leak elevates cytosolic Ca^{2+}, thereby mediating the increased miniature glutamate release seen
167 in our YAC128 cultures **(Figure 2A, B)**. To test this hypothesis, we first recorded mEPSCs before
168 and during local application of low dose (5 μM) ryanodine to cultured CPNs; 5 μM ryanodine
169 releases ER Ca^{2+} by opening ryanodine receptors (Meissner, 2017). In WT cultures, 5 μM
170 ryanodine nearly doubled the CPN mEPSC frequency: from 6.74 ± 1.17 Hz to 11.91 ± 2.36 Hz
171 [Students' paired T-test; p=0.0280; n=13 cells] **(Figure 2C - E)**. In YAC128 cultures, however,
172 ryanodine (5 μM) did not significantly alter the CPN mEPSC frequency: 11.98 ± 1.66 Hz vs 13.89
173 ± 2.01 Hz - under control conditions and in ryanodine (5 μM) respectively **(Figure 2F - H)**. A
174 Comparison of the percent change in mEPSC frequency following ryanodine (5 μM) revealed a
175 significantly greater response in WT than in YAC128 CPNs [31.7 ± 7.5 % (n=13) vs 5.2 ± 9.5 %
176 (n=15) in WT and YAC128 CPNs respectively (Students' unpaired T-test; p=0.0418)]. We next
177 used caffeine (1 mM) as an alternative means of agonizing ryanodine receptors; this more
178 prominently increased the mEPSC frequency in WT cultures, but otherwise produced similar
179 results **(Supplemental Figure 2)**.
180
181

182 **Removing extracellular Ca^{2+} and blocking the ER SERCA pump substantially reduces the**
183 **mEPSC frequency in YAC128 but not WT cultures**
184
185 If an ongoing release of presynaptic ER Ca^{2+} in YAC128 cultures occludes potentiation of synaptic
186 glutamate release by low dose ryanodine and caffeine, blocking ER Ca^{2+} release should reduce
187 synaptic glutamate release in YAC128 cultures. To test this, we pre-incubated cultures with
188 extracellular fluid (ECF) containing the sarco/endoplasmic reticulum Ca^{2+}-ATPase (SERCA)
189 pump inhibitor cyclopiazonic acid (CPA) (30 μM) to deplete ER Ca^{2+} stores. Since ER Ca^{2+}
190 depletion can increase cytosolic Ca^{2+} by engaging the store operated Ca^{2+} response, and this effect
191 can increase mini neurotransmitter release (Emptage et al., 2001), we performed these experiments
192 in the absence of extracellular Ca^{2+}. Under these conditions, YAC128 CPNs showed a mean
193 mEPSC frequency of 3.33 ± 0.57 Hz (n=14), significantly lower than seen in WT CPNs under
194 identical conditions 8.41 ± 1.50 Hz (n=17) (Student's unpaired t-test; p=0.0062) **(Figure 2I-K)**.
195 These results suggest that an ER calcium leak into the cytoplasm elevates mini vesicular glutamate
196 release from YAC128 CPN terminals, and that in the absence of this effect, the intrinsic vesicular
197 release probability is actually reduced in YAC128 compared to WT cortical terminals.
198
199 **Presynaptic Ca^{2+} sparks and waves are more frequent in YAC128 cultures**
200
201 To directly monitor presynaptic Ca^{2+} dynamics, we next fused GCaMP6-M (T.-W. Chen et al.,
202 2013) with the rat synaptophysin protein via a small glycine-serine linker to generate a genetically-
203 encoded Ca^{2+} sensor that preferentially localizes to presynaptic terminals. We expressed this rat
204 synaptophysin-tagged GCaMP6-M construct (rSyph-GCaMP6m) in neurons in cortical cultures

205 and performed Ca^{2+} imaging experiments, first in the presence of TTX (500 nM) to relate
206 presynaptic Ca^{2+} signaling to our mEPSC findings (above). Remarkably, both YAC128 and WT
207 cultures showed spontaneous axonal Ca^{2+} sparks, often beginning in single boutons, then initiating
208 slow Ca^{2+} waves spreading to neighboring boutons **(Figure 3A, B)**. In some cases, the above waves
209 slowly traversed axons encompassing entire 63X (178.6 μm x 113.1 μm) imaging fields over
210 multiple seconds of imaging. Conversely, axonal Ca^{2+} events in the absence of TTX could not be
211 temporally resolved (owing to relatively slow GCaMP kinetics) and appeared simultaneously
212 across all the boutons of a given imaged axon. These mini presynaptic Ca^{2+} events in TTX were
213 also strikingly long lasting at individual boutons - on average 5 - 10 times longer than that of
214 typical events seen in the absence of TTX **(Figure 3C, D)**. These miniature presynaptic Ca^{2+} events
215 in TTX were more than three times as frequent in YAC128 cultures than in WT cultures **(Figure**
216 **3E)**, but event DF/F amplitudes did not significantly differ between genotypes **(Figure 3F)**. The
217 detection algorithm used here (see methods) considered Ca^{2+} waves involving multiple axonal
218 boutons as single events (as in **Figure 3A**). However, the mean event area was similar in both
219 genotypes (not illustrated), suggesting similar numbers of axonal boutons were recruited on
220 average by such events in YAC128 and WT cultures. In subsets of WT and YAC128 cultures we
221 also expressed an mCherry-tagged PSD95 construct. In these cultures, we repeatedly observed
222 clear colocalizations between rSyph-GCaMP6m-labeled boutons, spontaneously active in TTX,
223 and mCherry-labeled dendritic spines (not illustrated). Thus although we cannot be certain that all
224 boutons showing spontaneous Ca^{2+} events in TTX participate in synaptic connections, it is clear
225 that such events are not restricted to ectopic boutons.
226
227

228 **Basal cytosolic Ca^{2+} is higher in YAC128 presynaptic boutons**

229

230 In a subset of TTX experiments, we applied the Ca^{2+} ionophore ionomycin (10 μM) to cultures
231 following GCaMP imaging. By equilibrating cytosolic Ca^{2+} to extracellular levels, this approach
232 allowed quantification of GCaMP fluorescence in the presence of the known extracellular Ca^{2+}
233 concentration (here 2 mM). Thus, smaller ionomycin-mediated increases in GCaMP fluorescence
234 indicate relatively higher basal (pre-ionomycin) cytosolic Ca^{2+} concentrations (Lindhout et al.,
235 2019). In both genotypes, ionomycin-mediated changes in presynaptic GCaMP fluorescence
236 (DF/F) were significantly smaller in boutons that had shown at least one spontaneous Ca^{2+} event
237 in the previous 3 min recording **(Figure 4A, D)**, indicating higher basal cytosolic Ca^{2+}
238 concentrations in these spontaneously active boutons. Furthermore, overall ionomycin responses
239 were significantly smaller in YAC128 cultures than in WT cultures when comparing the entire
240 population of boutons imaged in a culture (both spontaneously active and inactive) **(Figure 4E)**.

241

242 **Caffeine increases basal Ca^{2+} and miniature events in WT, but not YAC128 cortical boutons**

243

244 The slow kinetics of the above miniature presynaptic Ca^{2+} events are consistent with ER-mediated
245 Ca^{2+} waves reported in postsynaptic neuronal compartments (Ross, 2012). We next tested whether
246 these presynaptic Ca^{2+} events were affected by caffeine (1 mM), an ER ryanodine receptor agonist
247 that substantially increased mEPSC frequencies in WT, but not YAC128 cultures (above). In the
248 presence of TTX, caffeine (1 mM) significantly increased the presynaptic Ca^{2+} event frequency in
249 WT cultures **(Figure 5A)**, but did not significantly alter event frequency in YAC128 cultures
250 **(Figure 5B)**.

251

252 Significant photobleaching of the rSyph-GCaMP6m construct occurred with prolonged imaging;
253 this combined with the relative infrequency of mini presynaptic Ca^{2+} events necessitated imaging
254 of separate fields for the above control and caffeine comparisons. We next performed within-
255 bouton measurements of basal rSyph-GCaMP6m fluorescence before and immediately following
256 application of caffeine; the relatively short duration of these experiments made before and after
257 measurements feasible. A clear slow increase in basal rSyph-GCaMP6m fluorescence was seen in
258 most WT boutons following caffeine (1 mM) application **(Figure 5C)**, which was generally absent
259 or reduced in YAC128 boutons **(Figure 5D)**. Overall a significantly greater caffeine (1 mM)-
260 mediated increase in rSyph-GCaMP6m fluorescence was seen in WT boutons compared to
261 YAC128 **(Figure 5E)**.

262

263

264 **Action potential-dependent Ca^{2+} signals in presynaptic cortical terminals Are less frequent**
265 **in YAC128 cultures**

266

267 We next used the rSyph-GCaMP6m construct in the absence of TTX to examine presynaptic action
268 potential-dependent Ca^{2+} signals in WT and YAC128 cortical cultures. When neuronal action
269 potential firing was intact, rSyph-GCaMP6m -expressing boutons in both WT and YAC128
270 cultures were dominated by presumably voltage-gated Ca^{2+} channel-mediated signals **(Figure 6A,**
271 **B)**. These signals were more frequent than those seen in the presence of TTX, but of far shorter
272 duration. Interestingly, these activity-dependent Ca^{2+} events were nearly twice as frequent in WT
273 axonal boutons, compared to those in YAC128 cultures **(Figure 6A, C and E).** Ryanodine (5 μM)

274 modestly but significantly reduced the frequency of these events in WT cultures (by 17 %) **(Figure**
275 **6A, B and E)**. Conversely, 5 μM ryanodine elicited a modest, but significant increase in the
276 frequency of these events in YAC128 cultures **(Figure 6C- E)**.
277
278 As discussed above, rSyph-GCaMP6m events in the presence of TTX were typically much longer
279 in duration than action potential-dependent events in both genotypes and appeared to be restricted
280 to a subset of boutons with higher resting Ca^{2+} concentrations. Interestingly, similar strikingly
281 long-lasting events continued to occur in subsets of boutons in the absence of TTX. In an attempt
282 to identify boutons exhibiting these slow Ca^{2+} events, we next categorized boutons imaged in the
283 absence of TTX based on whether one or more Ca^{2+} events with a duration greater than 6 s
284 (measured at half peak amplitude) occurred during a 3 min recording. 6 s was chosen as the cutoff
285 value, because it was more than 5 standard deviations greater than the mean event duration seen
286 in WT and YAC128 boutons in the absence of TTX, but comparable to average event durations in
287 TTX in both genotypes: [8.60 ± 0.92 s (n=164) and 6.23 ± 0.35 s (n=440) in WT and YAC128
288 boutons respectively]. Without TTX, 7.9 % (23/292) of WT boutons showed one or more events
289 lasting longer than 6 s, while under identical conditions 10.4 % (44/423) of YAC128 boutons
290 showed at least one such event. Interestingly in both genotypes, overall event frequencies were
291 significantly lower in boutons showing one or more slow events (>6 s) than in boutons showing
292 only short duration events **(Figure 6F- I)**. Assuming boutons displaying these long lasting Ca^{2+}
293 events correspond to the same population that is spontaneously active in TTX, these results suggest
294 action potential-dependent Ca^{2+} events are reduced in the bouton population with higher resting
295 cytosolic Ca^{2+} levels and spontaneous ER release events. Taken together, experiments up to this
296 point suggest that releasing presynaptic ER Ca^{2+} elevates miniature vesicular glutamate release,

297 but can also reduce activity-dependent presynaptic Ca^{2+} influx, and imply that the spontaneous or
298 pharmacological release of presynaptic ER Ca^{2+} oppositely regulates miniature and action
299 potential-dependent glutamate release.
300
301 **Low dose ryanodine reduces evoked glutamate release in WT- but not YAC128-derived**
302 **brain slices**
303
304 We next performed experiments in cortical-striatal *ex-vivo* brain slices prepared from 2 – 3 month
305 old WT and YAC128 mice expressing the fluorescent glutamate sensor iGluSnFR in striatal
306 neurons (Parsons et al. 2016; Koch et al. 2018). This preparation allowed direct optical
307 measurement of glutamate release in the striatum, independent of postsynaptic neuronal properties.
308 Striatal iGluSnFR signals evoked by stimulating cortical axons of the corpus callosum were
309 significantly decreased by ryanodine (5 μM) in WT, but not YAC128 slices **(Figure 7)**. These data
310 are consistent with results in culture (Figs. 6), suggesting that AP-dependent glutamate release is
311 reduced in YAC128 as a consequence of a tonic Ca^{2+} leak from ER stores
312
313 **Discussion**
314
315 Presynaptic neurotransmitter release and consequent postsynaptic signaling largely underlies
316 communication between neurons, thus forming the basis of brain circuitry. Neurotransmitter
317 release in turn, can be broadly divided into action potential-dependent or independent forms. The
318 former requires presynaptic voltage-gated Ca^{2+} channel activation coordinated by sodium action
319 potentials; while the latter persists in the absence of neuronal activity. Although miniature

320 neurotransmission is poorly understood compared to its activity-dependent counterpart, it is
321 increasingly accepted to subserve clear physiological functions (Frank, Kennedy, Goold, Marek,
322 & Davis, 2006; McKinney, Capogna, Dürr, Gähwiler, & Thompson, 1999; Sutton et al., 2006).
323 Moreover, miniature release can be regulated relatively independently of action potential-
324 dependent release and may even be mediated by distinct vesicular pools (Fredj & Burrone, 2009;
325 Sara, Virmani, Deák, Liu, & Kavalali, 2005).
326
327 Alterations in synaptic signaling processes, particularly relating to the excitatory transmitter
328 glutamate, have been repeatedly reported in models of HD (Raymond et al., 2011; Sepers et al.,
329 2017; Tyebji & Hannan, 2017) and other neurodegenerative diseases (R. Wang & Reddy, 2017).
330 Increased cell-surface expression of extra-synaptic NMDA receptors by SPNs favors excitotoxic
331 postsynaptic glutamate-mediated signaling in HD models (Milnerwood et al., 2010). Mounting
332 evidence also suggests glutamate release from cortical afferents is altered in HD; however, the
333 direction of this alteration appears to be disease-stage-dependent (Cepeda et al., 2003; Joshi et al.,
334 2009).
335
336 The endoplasmic reticulum (ER), a continuous intracellular membrane-system involved in Ca^{2+}
337 storage and protein synthesis, is expressed in all neuronal processes including axons and
338 presynaptic boutons. Increased cytosolic Ca^{2+}-release from the ER has been shown in HD models,
339 as a result of a mutant huntingtin protein (mHTT)-mediated increase in IP3 receptor
340 responsiveness (Tang et al., 2003) and a constituent ryanodine receptor Ca^{2+} leak (Suzuki et al.,
341 2012). Previous HD studies have focused on the postsynaptic ER, however Ca^{2+} release from the
342 presynaptic ER is known to modulate neurotransmitter release (Emptage et al., 2001; Llano et al.,

343 2000). Results of our study suggest mHTT expression alters ER Ca^{2+} handling at stores in close
344 proximity to cortical presynaptic terminals, thereby altering glutamate release. This mechanism
345 clearly increased the frequency of Ca^{2+}-dependent, action potential-independent (mini) synaptic
346 glutamate events in our YAC128 model. Conversely, our findings suggest reduced action
347 potential-dependent glutamate release from YAC128 cortical terminals. As we have focused
348 exclusively on glutamatergic synapses, future experiments will be required to determine if this
349 mechanism similarly affects the release of other neurotransmitters and neuromodulators.
350
351
352 **Spontaneous axonal Ca^{2+} signaling increases the YAC128 miniature glutamate release**
353 **frequency**
354
355 CPNs in YAC128 cortical cultures at DIV14 and DIV18 showed higher mEPSCs frequencies
356 compared to CPNs in age-matched WT cultures. However by DIV 21, mEPSC frequencies were
357 similar between WT and YAC128 CPNs. This pattern is reminiscent of SPN mEPSC frequencies
358 in YAC128 cortical-striatal co-cultures, which were also higher relative to WT at early DIV ages,
359 but comparable to WT by DIV21 (Buren et al., 2016). In the co-culture model, the total dendritic
360 length of YAC128 SPNs was reduced relative to WT at DIV21, indicating reduced total SPN
361 synapse numbers may have masked ongoing elevated glutamate release rates from individual
362 YAC128 cortical terminals. We suspect that in our cortical cultures, degenerative changes at
363 DIV21 likewise obscured the elevated YAC128 CPN mEPSC frequencies clearly seen at earlier
364 DIV ages. Notably in DIV18-aged cortical cultures, the time point at which we performed
365 mechanistic experiments, no genotype differences in CPN synapse density and dendritic

366 morphology were evident, indicating that differences in mEPSC frequencies likely reflected
367 altered rates of release at individual presynaptic sites. In any case, increased rates of miniature
368 glutamate release appear to be an early and perhaps enduring phenotype of cultured YAC128
369 CPNs.
370
371 Caffeine or low dose ryanodine, which release ER Ca^{2+} by opening ryanodine receptors, failed to
372 increase the mEPSC frequency in YAC128 CPNs, despite robustly increasing the WT mEPSC
373 frequency. This result, in concert with the increased basal YAC128 mEPSC frequency, suggests
374 an ongoing spontaneous Ca^{2+} store release in YAC128 cultures occludes facilitation of the mEPSC
375 frequency by drug-mediated Ca^{2+} store release. The substantially lower CPN mEPSC frequency
376 seen in YAC128 cultures incubated with the ER SERCA pump inhibitor CPA in nominally zero
377 extracellular Ca^{2+}, is also consistent with a strong ER-derived Ca^{2+}-dependence of YAC128 mini
378 glutamate release. Conversely, mEPSC frequencies in WT cultures were not substantially reduced
379 under identical conditions; this resulted in significantly higher WT than YAC128 mEPSC
380 frequencies in CPA and 0 mM extracellular Ca^{2+}, notably opposite the relationship seen without
381 CPA in standard (2 mM) extracellular Ca^{2+}. This was unexpected given overall WT and YAC128
382 CPN synapse numbers were similar in these cultures, but may indicate a reduction in functional
383 YAC128 synapses, not apparent in fixed culture images, or deficits in the YAC128 synaptic release
384 machinery, as suggested in previous studies (Morton & Edwardson, 2001; Morton, Faull, &
385 Edwardson, 2001). In either case, enhanced Ca^{2+}-dependent mini glutamate release in YAC128
386 cultures clearly surmounts any such deficits. These results also suggest mini glutamate release in
387 WT cultures is largely Ca^{2+}-independent. In contrast, Xu et. al (2009) reported mini glutamate
388 release in similar cortical cultures persisted in the absence of extracellular Ca^{2+}, but was nearly

389 completely dependent on internal Ca^{2+}stores and blocked by preincubation with the membrane-
390 permeant Ca^{2+} chelator BAPTA-AM (Xu, Pang, Shin, & Südhof, 2009). If this were true in our
391 cultures, we would expect Ca^{2+} store depletion (with CPA), in concert with removal of extracellular
392 Ca^{2+}, to similarly abolish mini release. However CPA is reported to only partially deplete
393 presynaptic ER Ca^{2+} (de Juan-Sanz et al., 2017), therefore a role of residual ER Ca^{2+} in maintaining
394 mini release in WT cultures under these conditions cannot be excluded.
395
396 Despite a clear role of ER Ca^{2+} in mini release in a variety of neuronal preparations, the temporal
397 and spatial dynamics of action potential-independent presynaptic ER Ca^{2+} signals are largely
398 unclear. Imaging the rSyph-GCaMP6m probe in TTX revealed spontaneous, presynaptic Ca^{2+}
399 events that often initiated Ca^{2+} waves traversing cortical axons. These events were more frequent
400 in YAC128 cultures and showed strikingly slow kinetics in both genotypes, consistent with ER
401 Ca^{2+} waves reported in dendrites and non-neuronal cell-types (Ross, 2012). Caffeine substantially
402 increased the mini axonal Ca^{2+} event frequency in WT cultures to levels comparable to that seen
403 in YAC128 cultures, but failed to significantly change the event frequency in YAC128 cultures.
404 The congruence of these results with our mEPSC findings (above) suggests these axonal Ca^{2+}
405 events underlie the increased YAC128 mini glutamate release frequencies.
406
407 Basal cytosolic Ca^{2+} concentrations were higher in axonal boutons showing spontaneous Ca^{2+}
408 activity in TTX, compared to inactive boutons, in both genotypes. Elevated cytosolic Ca^{2+} levels
409 may therefore be required to precipitate the initial ryanodine or IP3 receptor opening needed to
410 incite the regenerative ER Ca^{2+}-induced Ca^{2+} release we presume underlie these axonal Ca^{2+}
411 events. Interestingly, the restriction of spontaneous Ca^{2+} signals to a subset of cortical boutons

412 with higher basal Ca^{2+} concentrations may mean mini glutamate release is not uniform across
413 cortical boutons, but favored from this population of spontaneously active boutons. Indeed,
414 subpopulations of synapses favoring mini release have been described in other neuronal systems
415 (Atasoy et al., 2008; Peled, Newman, & Isacoff, 2014; Reese & Kavalali, 2016). We suspect the
416 higher basal cytosolic Ca^{2+} concentrations in the overall YAC128 axonal bouton population meant
417 a greater proportion were capable of sustaining spontaneous Ca^{2+} activity. Caffeine application
418 increased the baseline cytosolic Ca^{2+} concentration and frequency of spontaneous events in WT,
419 but not YAC128 boutons, consistent with this idea.
420
421
422 **Action potential-dependent glutamate release is suppressed due to presynaptic ER depletion**
423
424 Regardless of genotype, striking differences were seen in the rSyph-GCaMP6m signals that
425 predominated in the presence versus absence of TTX. Most rSyph-GCaMP6m-expressing boutons
426 in the absence of TTX showed numerous spontaneous events during standard 3 min imaging
427 sessions. However, only subsets of boutons were spontaneously active in TTX, with active boutons
428 characterized by higher resting cytosolic Ca^{2+} concentrations. Furthermore, although Ca^{2+} events
429 at individual boutons in TTX were less frequent, they lasted many times longer than corresponding
430 action potential-dependent events. Interestingly in the absence of TTX, subsets of boutons of both
431 genotypes showed longer-lasting Ca^{2+} events, like those that persisted in TTX, typically alongside
432 faster action potential-dependent events. We suspect these boutons correspond to the population
433 spontaneously active in TTX. Event frequencies in such boutons, in the absence of TTX, were
434 significantly lower than in boutons lacking these longer-lasting events, further supporting the idea

435 that subsets of cortical boutons favor either miniature or action potential-dependent glutamate
436 release.
437
438 Although spontaneous axonal Ca^{2+} events were more common in YAC128 cultures in the presence
439 of TTX, the opposite was true when experiments were performed without TTX, suggesting
440 reduced activity-dependent glutamate release in YAC128 cultures. Reduced action potential-
441 dependent axonal Ca^{2+} event frequencies in YAC128 cultures could reflect decreased CPN firing
442 rates, altered transduction of sodium action potentials to bouton Ca^{2+} signals or some combination
443 of these factors. 5 μM ryanodine significantly reduced the frequency of these action potential-
444 dependent bouton Ca^{2+} events in WT cultures, though not to YAC128 levels, consistent with
445 reduced action potential-dependent presynaptic Ca^{2+} signaling in YAC128 cultures being partly,
446 but not entirely mediated, by spontaneous release of ER Ca^{2+}. However, nuances of ryanodine's
447 pharmacology may have confounded this conclusion. Low dose ryanodine opens ryanodine
448 receptors, but to a sub-maximal conductance state. Furthermore, ryanodine binding to a second
449 low affinity receptor site mediates channel closure, an action that predominates at doses greater
450 than 10 μM. Caffeine more effectively releases ER Ca^{2+}, exemplified here in patch clamp mini
451 EPSC experiments, and may therefore have been capable of lowering action potential-dependent
452 event frequencies in WT to YAC128 levels. Unfortunately, caffeine was undesirable for these
453 experiments because, unlike ryanodine, it is an antagonist at adenosine receptors, which are often
454 expressed at presynaptic sites and inhibit VGCCs (Dunwiddie & Masino, 2001). We speculate that
455 the ryanodine receptor population in YAC128 boutons favors the open conformation under basal
456 conditions, consistent with the lack of caffeine responses in YAC128 boutons, and that under such
457 conditions, ryanodine-mediated channel closure would be exaggerated. If so, this could account

458 for the modest, but significant ryanodine-mediated increase in event frequencies in YAC128
459 boutons.
460
461 Precise mechanism(s) by which pharmacological or disease-mediated ER Ca^{2+} release might
462 reduce activity-dependent presynaptic Ca^{2+} signaling remain uncertain. Indeed axonal or cell body
463 ER stores could equally underlie this effect given the dependence of these signals on sodium action
464 potentials. Dendritic ryanodine receptor activation has been shown to reduce neuronal firing rates
465 via activation of a Ca^{2+}-dependent K^+ conductance (van de Vrede, Fossier, Baux, Joels, &
466 Chameau, 2007). Alternatively, elevated cytosolic Ca^{2+} levels in YAC128 boutons (mediated by
467 the release of axonal stores) might contribute to Ca^{2+}-dependent VGCC inactivation, thereby
468 reducing the coupling of cortical action potentials to presynaptic VGCC-mediated Ca^{2+} influx.
469 Indeed, more generalized increases in cytosolic Ca^{2+} mediated by ER store release, have been
470 shown to facilitate Ca^{2+}-dependent inactivation of voltage-gated Ca^{2+} channels including the N
471 and P/Q-types commonly expressed in presynaptic terminals and implicated in vesicular release
472 (Budde, Meuth, & Pape, 2002; Cens, Rousset, Leyris, Fesquet, & Charnet, 2006). If this were the
473 case in our system, the higher resting Ca^{2+} concentrations evident in YAC128 boutons would be
474 expected to maintain local voltage-gated Ca^{2+} channels in a higher resting state of inactivation.
475
476 Low-dose ryanodine decreased the amplitude of striatum, glutamate-mediated iGluSnFR signals
477 in WT brain slices, an effect absent or diminished in YAC128 slices, consistent with our findings
478 in culture. There is a lack of consensus as to whether single action potentials can trigger Ca^{2+}-
479 induced Ca^{2+} release from the presynaptic ER (Emptage et al., 2001), or whether prolonged,
480 repetitive action potential firing is required (de Juan-Sanz et al., 2017). It seems unlikely that the

481 stimulation protocol used here appreciably contributed to the action potential-dependent discharge
482 of the presynaptic ER, given the relatively low intensity stimulation used (repeated only twice at
483 100 Hz). Rather, we suspect a ryanodine-mediated increase in presynaptic Ca^{2+} decreased evoked
484 glutamate release by inactivating presynaptic voltage-gated Ca^{2+} channels in WT slices, and that
485 this process was occluded in YAC128 slices. However, future studies will be required to clarify
486 mechanistic details of this process.
487
488 Taken together, the evidence presented here strongly suggests enhanced spontaneous release of
489 presynaptic ER Ca^{2+} in YAC128 mice favors miniature glutamate release at the expense of evoked
490 release.
491
492 **Implications for postsynaptic signaling**
493 Mini glutamate release elicits postsynaptic NMDA receptor-mediated Ca^{2+} influx under
494 physiologically relevant conditions (Beaulieu-Laroche & Harnett, 2018; Espinosa & Kavalali,
495 2009) and can mediate postsynaptic signaling distinct from that of action potential-dependent
496 release (Sutton, Taylor, Ito, Pham, & Schuman, 2007). Indeed mini glutamate release may activate
497 distinct populations of NMDAR receptors (Atasoy et al., 2008). In cultures, it was reported that
498 miniature glutamate-mediated events become toxic to CPNs following prolonged silencing of
499 neuronal activity with TTX (Fishbein & Segal, 2007). Future studies will be necessary to
500 determine if and how the increased mini glutamate release shown here interacts with the well
501 described alterations in postsynaptic NMDA receptor expression in the YAC128 and other HD-
502 models, and whether a shift towards activity-independent glutamate release contributes to
503 neurodegeneration in HD.

504

505 **Materials and Methods**

506

507 **Culture preparation:**

508

509 All animal-related procedures were approved by and adhered to the guidelines of the University
510 of British Columbia Committee on Animal Care and the Canadian Council on Animal Care
511 (protocols A17-0295, A15-0069 and A19-0076). Cultures were prepared from both male and
512 female embryonic day 17-18 pups from either wild-type (WT) FVB/N or transgenic yeast artificial
513 chromosome-containing mice expressing the full-length human huntingtin genomic DNA with 128
514 CAG repeats (YAC128). YAC128 mice were maintained on the FVB/N background (homozygous
515 line 55). Wildtype and YAC128 mice used for ex vivo slice experiments (below) and bred for
516 culture preparation (above) were group housed under controlled conditions, free of know
517 pathogens, at room temperature (22 – 24 °C), under a 12 hr light/dark cycle. Cortical cultures used
518 in patch clamp electrophysiology and Ca^{2+}-imaging experiments were prepared as previously
519 described (Milnerwood et al., 2012; Smith-Dijak et al., 2019) and plated at a density of 225, 000
520 neurons/ml. In a subsets of experiments, a portion of the total 2.7 million cortical neurons (plated
521 per 24-well culture) were transfected with transgenic reporters including: GFP; a synaptophysin-
522 tagged GCaMP6-M construct (a generous gift from Dr. Anne Marie Craig, UBC); a postsynaptic
523 density 95 (PSD-95)–tagged M-cherry construct; or a GFP-tagged internally expressed anti-
524 PSD95 antibody (a generous gift from Dr. D.B. Arnold, University of Southern California; (Gross
525 et al., 2013)).

526

527

528 **Electrophysiology:**

529

530 An Axopatch 200B amplifier and pClamp 9.2 software (Molecular Devices, Sunnyvale, CA) were
531 used to acquire whole-cell patch clamp electrophysiology recordings. Data was digitized at 20 kHz
532 and low-pass filtered at 1 kHz. For electrophysiology experiments, cultures were perfused with
533 extracellular fluid (ECF) containing (in mM): 167 NaCl, 2.4 KCl, 10 glucose, 10 HEPES, 2 $CaCl_2$
534 and 1 $MgCl_2$; NaOH (1 mM) was used to adjust the pH to 7.30, and the osmolarity was adjusted
535 to 305 – 310 mOsm. Tetrodotoxin (TTX) (500 nM) and picrotoxin (PTX) (50 mM) were added to
536 this ECF to block sodium channel-mediated action potentials and $GABA_A$ receptor-mediated
537 currents respectively. Neurons were patched with borosilicate glass pipettes pulled to a tip
538 resistance of 3-6 MΩ when back-filled with intracellular solution containing in (mM): 130 Cs-
539 methanesulfonate, 5 CsCl, 4 NaCl, 1 MgCl, 10 HEPES, 5 EGTA, 5 QX-314 Cl, 0.5 Na-GTP, 10
540 Na-phosphocreatine, and 5 Mg-ATP (~286 mOsm). During experiments, neurons were held at –
541 70 mV in voltage-clamp, with hyperpolarizing voltage steps (-10 mV) performed periodically to
542 measure intrinsic membrane properties. Under these conditions AMPA receptor-mediated
543 miniature excitatory postsynaptic currents (mEPSC)s appeared as transient inward current
544 deflections. Recordings with a series resistance greater than 25 MΩ were excluded from analysis;
545 typical values were between 15 – 20 MΩ. A minimum of 2 minutes following establishment of the
546 whole cell configuration was allowed before experimental measurements, so neurons could fully
547 dialyze with intracellular solution and achieve a stable membrane resistance and holding current.
548 For experiments involving within-cell drug applications, a maximum 20 % change in series
549 resistance between control and drug measurements was tolerated. In these cases, drugs were

550 applied locally to the neuron with a fast perfusion system. Mini Analysis software (Synaptosoft)
551 was used to detect mEPSCs and extract relevant parameters. A minimum of 100 and no more than
552 1000 mEPSC's were analyzed per neuron per experimental condition.
553
554 **Cortical pyramidal neuron morphology:**
555

556 Cortical pyramidal neurons (CPN)s in WT and YAC128 cultures were labeled by transfecting a
557 subset of neurons (1 of 2.7 million) with a cytoplasmic green fluorescent protein (GFP)
558 (Addgene plasmid 37825) at the time of platting. Cultures were subsequently fixed at DIV17 - 19
559 and GFP-labeled CPN dendritic arbors imaged on a Zeiss Axiovert 200 M fluorescence
560 microscope (20 x magnification, 0.8 NA), with a Zeiss 702 monochrome camera, using Zen
561 software. Multiple image Z-stacks were acquired and X,Y-tiling was used to ensure entire dendritic
562 arbors were visualized. Images were exported to Fiji-ImageJ for analysis by a blinded observer.
563 Images were flattened using the maximum Z-projection function. Background subtraction was
564 performed, and neuronal processes were thresholded following adjustment of brightness and
565 contrast. Automated Sholl analysis was performed using the ImageJ sholl analysis plugin.
566
567 **Excitatory cortical synapse staining:**
568

569 A subset of neurons (2 of 2.7 million) in WT and YAC128 cortical cultures were transfected with
570 a GFP-tagged internally-expressed anti-PSD95 antibody (intrabody) (Gross et al., 2013) at the time
571 of platting. At DIV17 – 19, cells were fixed and stained for VGlut1 and the GluA2 AMPA receptor
572 subunit as previously described (Buren et al., 2016). Briefly, cultures were first live-stained with

573 a primary mouse anti-GluA2 antibody (Millipore), then fixed and stained with a secondary Alexa
574 Fluor 568-conjugated donkey anti-mouse antibody (Invitrogen). Subsequently, cultures were
575 incubated with a primary guinea pig anti-VGlut1 antibody (Millipore), then stained with a
576 secondary AMCA-conjugated donkey anti-guinea pig antibody (Jackson Immuno Research
577 Laboratories). To amplify the GFP fluorescence of the anti-PSD95 intrabody, cultures were also
578 incubated with a primary chicken anti-GFP antibody (1:1000) (Millipore), followed by an
579 secondary Alexa Fluor 488-conjugated antibody (1:500) (Invitrogen). Cultures were imaged on a
580 Zeiss Axiovert 200 M fluorescence microscope (63 x magnification, 1.4 NA), using a Zeiss 702
581 monochrome camera and Zen software. CPNs expressing the anti-PSD95 intrabody were
582 identified based on their diffuse cytoplasmic GFP fill, with bright GFP-labelled puncta expressed
583 at dendritic spines. A portion of each CPNs arbor, containing multiple secondary and tertiary
584 dendrites, was selected for imaging and sufficient image Z-stacks were acquired to adequately
585 capture all dendritic processes present in a given 63x field. Images were exported to Fiji-ImageJ
586 for analysis by a blinded observer and flattened using the maximum Z-projection function. For
587 each CPN image, the GFP channel was used to identify 3 secondary or tertiary dendritic segments,
588 at least 40 μm away from the CPN soma, over which ROIs were drawn. Following background
589 subtraction, fluorescent puncta in the green (GFP), red (Alexa Fluor 568) and blue (AMCA)
590 channels, visible within dendritic ROIs, were manually thresholded and detected with the analyze
591 particles function. The ImageJ colocalization plugin was used to identify triple-colocalized puncta
592 (PSD95, GluA2 and VGlut1), which we interpreted as functional CPN glutamatergic synapses.
593 Synapse density was defined as the number of triple-colocalized puncta present within a dendritic
594 segment divided by the area of the segment and averaged across all 3 dendrites analyzed in a given
595 CPN.

596

597 **Synaptophysin-GCaMP imaging:**

598

599 To directly image cytosolic Ca^{2+} in axonal boutons of neurons in our cortical mono cultures we
600 transfected 1 million cells (of a total 2.7 million) at time of plating with a rat synaptophysin-tagged
601 GCaMP6-M construct (rSyph-GCaMP6m). The rSyph-GCaMP6m construct was created by fusing
602 GCaMP6-M (T.-W. Chen et al., 2013) with the full length rat synaptophysin protein (1 – 307
603 amino acids) via a small glycine-serine linker and inserting the fused rSyph-GCaMP6-M construct
604 into a pLL3.7-hSyn vector to achieve neuron-selective expression. For some experiments, the same
605 1 million cells were also transfected at time of platting with an M-cherry-tagged PSD95 construct;
606 in these cases, rSyt-GCaMP6m-expressing presynaptic boutons that colocalized with M-Cherry
607 labeled postsynaptic spines were presumed to be functional synapses.

608

609 For all Ca^{2+}-imaging experiments, cultures were plated on 8-well cover-glass chambers (Thermo
610 Scientific ™, Nunc ™, Lab-Tek ™) and imaged at DIV (17 - 19) with a Zeiss Axiovert 200 M
611 fluorescence microscope (63 x magnification, 1.4 NA), using a Zeiss 702 monochrome camera
612 and Zen software. Movies were acquired at 10 Hz (100 ms exposure per frame) using the Zen
613 time-series mode with camera-steaming enabled. These experiments were performed in standard
614 ECF (as above) with or without TTX (500 nM) present, but in the absence of PTX.

615

616 Spontaneous Ca^{2+} waves were commonly observed in rSyph-GCaMP6m-labelled axons, evident
617 particularly when action potential-dependent Ca^{2+} events were blocked with TTX. Automatically
618 detecting such Ca^{2+} waves proved difficult with algorithms commonly used to quantify activity-

619 related neuronal GCaMP signals. We therefore used the Astrocyte Quantitative Analysis (AQuA)
620 software (running in MATLAB) (Y. Wang et al., 2019) to quantify these waves in the presence of
621 TTX. AQua does not rely on spatially segmenting a Ca^{2+} movie into ROIs based on neuronal
622 morphology, but rather defines events as spatially and temporally connected Ca^{2+} signals
623 surpassing user-defined thresholds. This means spontaneous axonal waves spreading across
624 multiple boutons are typically classified as a single event, because such Ca^{2+}-activity is grouped
625 in time and space. Conversely, a given bouton can be involved in multiple axonal waves and thus
626 detected as part of multiple events, as long as the pertinent signals are sufficiently temporally
627 separated. To compare the frequency of aQua-detected spontaneous axonal events between
628 genotypes and under pharmacological manipulations, we counted numbers of events occurring
629 within a standardized area [178.6 μm x 113.1 μm (a maximal 63 x field of view)], during a
630 standardized (3 min) consecutive imaging interval. The same aQua detection parameters,
631 empirically determined to best match a small number of manually analyzed experiments, were
632 applied across all cultures and conditions analyzed to facilitate meaningful comparisons.
633
634 In a subset of experiments conducted in the presence of TTX, responses of individual WT or
635 YAC128 rSyph-GCaMP6m-labelled synaptic boutons to caffeine or ionomycin were measured. In
636 these experiments culture fields were imaged for 3 min (as above), after which caffeine (1 mM) or
637 ionomycin (10 μM) was applied and imaging continued for an additional 1-2 min. aQua was not
638 used to analyze these experiments, as an ROI-based algorithm was desired. For caffeine
639 applications, an analyzer (blinded to culture genotype) used Fiji-ImageJ (NIH) to manually assign
640 elliptical ROIs to 10 boutons per movie and exported each ROI's fluorescence-intensity time-
641 course. Time-courses were subsequently imported to MATLAB, where the curve fitting tool was

642 used to model each time-course's photobleaching profile based on the initial 3 min recording; this
643 curve was then extrapolated to the entire time-course including caffeine treatment. The resultant
644 "bleaching curve" was subtracted from the raw rSyph-GCaMP6m fluorescence curve and this
645 time-course subsequently divided by the "bleaching curve" to yield a final curve reflecting the
646 caffeine response in DF/F units. Ionomycin experiments were analyzed similarly, except in this
647 case, the blinded analyzer selected 10 active-boutons (showing at least 1 clear Ca^{2+} event during
648 the initial 3 min recording) and 10 inactive-boutons (with no Ca^{2+} events present during the initial
649 3 min recording). Time-courses derived from inactive-boutons were exported to MATLAB, where
650 the ionomycin-mediated DF/F responses were calculated as above. In the case of active-boutons,
651 spontaneous events occurring during the first 3 min were detected with MATLAB's findpeaks
652 function and excised from the raw fluorescence time-courses before curve fitting, but otherwise
653 processed as above.
654
655 As expected, spontaneous events were far more frequent when rSyph-GCaMP6m -expressing
656 cultures where imaged in the absence of TTX. Most boutons showed many events during a 3 min
657 imagining session. These events, which were presumably driven by the action potential-dependent
658 opening of voltage-gated Ca^{2+} channels, were far shorter in duration than typical TTX-resistant
659 events. To assess for genotype differences in these signals, a blinded analyzer used Fiji-ImageJ to
660 randomly assign elliptical ROIs to 20 boutons per movie and exported each ROI's fluorescence-
661 intensity time-course to MATLAB. The high frequency of action potential-dependent events often
662 precluded extracting the photobleaching profile of a bouton's time-course, necessitating an
663 alternative means of calculating the DF/F values of spontaneous events. We therefore averaged
664 the grey-value fluorescence intensity across an entire-time course, subtracted this average

665 fluorescence pointwise from the time-course, then divided pointwise by the average fluorescence
666 to convert to DF/F units. Any nonstationary present in these DF/F time-series due to
667 photobleaching was removed with the MATLAB detrend function. The MATLAB findpeaks
668 function was subsequently used to detect events in these DF/F traces and extract relevant
669 parameters including peak event DF/F amplitudes and event half-amplitude widths. Bouton event
670 frequencies were calculated by dividing numbers of detected events in a DF/F trace by the imaging
671 interval. Bouton event frequencies and event parameters in the absence of TTX were compared
672 between WT and YAC128 cultures under baseline conditions and following application of
673 ryanodine (5 μM).
674
675 **iGluSnFR imaging in acute brain slices:**
676
677 Expression of the genetically-encoded intensity-based glutamate-sensing fluorescence reporter
678 (iGluSnFR) (Marvin et al. 2013) in WT and YAC128 mice was achieved with stereotaxic injection
679 of a viral construct as described previously (Parsons et al., 2016). Briefly, under isoflurane
680 anesthesia, 1 – 1.4 μl of the AAV1.hSyn.iGluSnFr.WPRE.SV40 construct (Penn Vector Core; Dr.
681 Loren Looger, Janelia Farm Research Campus of the Howard Hughes Medical Institute) was
682 directly injected into the dorsal striatum of 4 – 6 week old mice. Following surgery, mice were
683 closely monitored for a week to ensure adequate recovery.
684
685 After waiting 3 – 6 weeks, to ensure optimal iGluSnFR expression, acute brain slices from 2-3
686 month-old YAC128 mice and age-matched WT controls were prepared as described previously
687 (Parsons et al., 2016; Koch et al., 2018). Briefly, mice were decapitated following deep

688 isoflurane anesthesia and their brains rapidly removed and placed in an ice-cold slicing solution,
689 bubbled with carbogen (95% O_2, 5% CO_2) gas, containing (in mM): 125 NaCl, 2.5 KCl, 25
690 $NaHCO_3$, 1.25 NaH_2PO_4, 2.5 $MgCl_2$, 0.5 $CaCl_2$, and 10 glucose. 300 μm thick striatum-containing
691 sagittal brain slices were cut with a Leica VT1200S vibratome. Slices were subsequently incubated
692 for 30 min in warmed artificial cerebral spinal fluid ACSF containing 2 mM $CaCl_2$ and 1 mM
693 $MgCl_2$; ACSF constituents and concentrations were otherwise identical to the slicing solution
694 (above).
695
696 Slices were transferred to a submerged recording chamber for experiments and perfused with
697 carbogen-bubbled ACSF at a rate of 2 – 3 ml/min at room temperature. Cortical release of
698 glutamate into the striatum was evoked by delivering paired 0.1 ms electrical pulses at 100 Hz
699 with an A-M Systems isolated pulse stimulator (Model 2100) and tungsten monopolar stimulating
700 electrode (tip resistance - 0.1 MΩ). The electrode was placed into a corpus callosum segment
701 adjacent to the dorsal striatum at an approximate 50 – 100 μm depth. During and immediately prior
702 to the electrical stimulation, iGluSnFR fluorescence was excited with a 470 nm LED; slices were
703 not illuminated between experimental measurements to minimize phototoxicity and bleaching.
704 Stimulation and LED activation were triggered by Clampex software (Molecular Devices,
705 Sunnyvale, CA). iGluSnFR fluorescence was isolated with a 530 nm bandpass filter and imaged
706 with a CCD camera (1 M60, Pantera, Dalsa) and XCAP software (Epix, inc.) at 150 Hz with 8 x
707 8-pixel binning. Experimental measurements encompassing four stimulation trials and two blank
708 trial were performed at 3-minute intervals. The four stimulation trials were averaged and the blank
709 trials, in which slice-fluorescence was imaged without electrical stimulation, were averaged and
710 used to account for photobleaching and to calculate the stimulation mediated changes in iGluSnFR

711 fluorescence over basal fluorescence (ΔF/F) as described previously (Parsons et al., 2016).
712 Videos were analyzed offline with ImageJ software. The average iGluSnFR signal was measured
713 over 10 x 10-pixel (93.8 x 93.8 μM) region of interested (ROI) placed over the maximal area of
714 evoked iGSnFR activity within the striatum adjacent to the stimulating electrode.
715
716 **Experimental design and statistical analysis:**
717
718 Statistical analysis and creation of figures was performed using GraphPad Prism (version 7). All
719 data distributions were tested for normality with the D'Agostino-Pearson omibus normality test.
720
721 The Student's unpaired t-test was used for unpaired comparisons between two data groups, such
722 as when mean mEPSC frequencies were compared between WT and YAC128 neurons, as long
723 both data groups were normally distributed. When one or both groups failed the D'Agostino-
724 Pearson omibus normality test, the non-parametric Mann Whitney test was used instead.
725
726 When parameters of the same group of neurons or axonal boutons were compared before and after
727 a drug treatment, statistical significance was assessed with the Student's paired t-test, unless data
728 points in the control or drug-treatment group failed the D'Agostino-Pearson omibus normality test;
729 in which case, the non-parametric Wilcoxon matched-pairs signed rank test was used instead.
730
731 A two-way ANOVA with the Bonferroni post-test was used when testing for genotype differences
732 in a dependent variable measured at different time points, as was the case for our brain-slice
733 iGluSnFR experiments.

734

735 Depending on the experimental design, “n” numbers in figures refer either to number of neurons,
736 numbers of imaged culture fields, numbers of individual axonal boutons, or numbers of brain
737 slices. Clarifying details are present within individual figure legends, as are the numbers of culture
738 batches or mice used.

739

740 Differences in mean values were considered significant at $p<0.05$, and significance levels are
741 indicated in figures as follows: *$p<0.05$, **$p<0.01$, ***$p<0.001$, ***$p<0.0001$. Comprehensive
742 descriptions of statistical analysis are included in figure legends.

743

744 **Acknowledgments**

745

746 We thank Dr. Anne Marie Craig (UBC) for expert advice on experiments using rSyph-GCaMP6m,
747 and Dr. Lily Zhang and Dr. Rujun Kang for technical support and assistance. The work was
748 supported by funding from the Canadian Institutes of Health Research (CIHR) Foundation grants
749 FDN-143210 to LAR and FDN-154278 to MRH. CB was supported by a University of British
750 Columbia 4-year Graduate Fellowship (UBC 4-YF). ASD was supported by a CIHR Canada
751 Graduate Scholarship Doctoral award and a UBC 4-YF. EK was supported by a CIHR Canada
752 Graduate Scholarship Master’s award and UBC 4-YF. MES was supported by a Vanier Canada
753 Graduate Scholarship and a UBC 4-YF. WN was supported by a UBC-CIHR-MD/PhD studentship
754 and a Vanier Canada Graduate Scholarship. LAR holds the UBC Department of Psychiatry Louise
755 A. Brown Chair in Neuroscience. MRH holds a Canada Research Chair.

756

Declaration of Interests

The authors declare no competing interests.

780 **Figure legends:**

781

782 **Fig 1: YAC128 cortical cultures show elevated miniature EPSC frequencies at early DIV**
783 **time points.**

784 Representative traces (**A, D, G, J**) and population data for mEPSCs (frequency in **B, E, H, K**;
785 amplitude in **C, F, I, L**) recorded from WT and YAC128 CPNs. All recordings were made in
786 voltage clamp with a holding potential of -70mV in solution containing TTX (500 nM) and PTX
787 (50 μM).

788 **A – C:** Recordings made from CPNs in DIV-7 cultures**.** Mean mEPSC frequency (**B**) was 1.8 ±
789 0.3 Hz (n=18; 3 cultures) in WT CPNs and 2.8 ± 0.7 Hz (n=17; 4 cultures) in YAC CPNs; this
790 difference was not statistically significantly [t(33)=1.449; p=0.1567; Student's unpaired-t test].
791 Mean mEPSC amplitudes (**C**) were similar in WT and YAC128 cultures: 17.2 ± 1.5 pA (n=18; 3
792 cultures) and 17.0 ± 1.7 pA (n=17; 4 cultures) respectively [t(33)=0.06936; p=0.9452; Student's
793 unpaired-t test].

794 **D - F:** Recordings were made from CPNs in DIV-14 cortical cultures. Mean mEPSC frequency
795 (**E)** was significantly higher in YAC128 CPNs [10.8 ± 1.8 Hz (n=20; 6 cultures)] compared to WT
796 CPNs [4.4 ± 2.6 Hz (n=22; 4 cultures)], [t(40)=3.555; p=0.0010; Student's unpaired-t test]. Mean
797 CPN mEPSC amplitudes (**F**) were not significantly different in WT and YAC128 cultures: 12.1 ±
798 0.8 pA (n=22; 4 cultures) and 15.0 ± 1.4 pA (n=20; 6 cultures), respectively [t(40)=1.807;
799 p=0.0786; Student's unpaired-t test].

800 **G – I:** Recordings were made from CPNs in DIV-18 cortical cultures. Mean CPN mEPSC
801 frequency (**H**) was significantly higher in YAC128 cortical cultures [14.1 ± 1.2 Hz (n=38; 10
802 cultures)] compared to WT cultures [9.9 ± 1.5 Hz (n=30; 15 cultures)], [p<0.0059 (exact); Mann

803 Whitney test]. Mean CPN mEPSC amplitudes (**I**) were similar in WT and YAC128 cultures: 17.0
804 ± 1.8 pA (n=30; 15 cultures) and 17.4 ± 1.8 pA (n=38; 10 cultures) respectively [p=0.8643 (exact);
805 Mann Whitney test].
806 **J – L:** Recordings were made from CPNs in DIV-21 cortical cultures. Mean CPN mEPSC
807 frequency (**K**) was similar in WT and YAC128 cultures: 14.2 ± 1.2 Hz (n=62; 17 cultures) and
808 14.0 ± 0.9 Hz (n=71, 23 cultures), respectively [p=0.5626 (exact); Mann Whitney test]. Mean CPN
809 mEPSC amplitudes (**L**) were similar in WT and YAC128 cultures: 22.3 ± 1.3 pA (n=62; 17
810 cultures) and 24.3 ± 1.2 pA (n=71; 23 cultures), respectively [p=0.2143 (exact); Mann Whitney
811 test].
812
813 **Supplemental Fig 1: Dendritic complexity and excitatory synapse numbers are similar in**
814 **WT and YAC128 cortical cultures.**
815 **A, B.** Representative images generated by thresholding a merged Z-stack of a green fluorescent
816 protein (GFP)-expressing WT CPN (**A**) and YAC128 CPN (**B**).
817 **C.** Number of dendritic intersections through concentric sholl circles centered on the soma of GFP-
818 filled WT and YAC128 CPNs of radii between 10 μm and 450 μm. WT and YAC128 CPNs have
819 nearly identical dendritic branching distributions [2-way ANOVA; Genotype: F(1, 6165)= 1.168,
820 p<0.2799; Distance from soma: F(44, 6165)=381.6, p<0.0001; Interaction: F(44, 6165)=0.9868,
821 p<0.4966].
822 **D.** Total numbers of sholl intersections, which reflect general neuronal complexity, were similar
823 in WT and YAC128 CPNs: 254.0 ± 8.8 (n=61; 4 cultures) and 249.5 ± 8.7 (n=78; 4 cultures)
824 respectively [p=0.7263 (exact); Mann Whitney test].

825 **E.** A representative merged Z-stack from a WT CPN (left panels) and YAC128 CPN (right panels)
826 with merged green, red and blue channels showing staining of a genetically-encoded internally-
827 expressed GFP-tagged anti-PSD-95 antibody (green), anti AMPA receptor GluA2 subunit
828 immuno-staining (red) and anti VGlut1 immuno-staining (blue) respectively. The bottom panel
829 shows an expanded view of a segment of dendrite with arrows pointing to a subset of co-localized
830 PSD-95, GluA2 and VGlut1 puncta, which were counted as presumed functional synapses. Note,
831 for illustrative purposes the brightness and contrast of the individual channels were adjusted to
832 best illustrate the punctate fluorescence.
833 **F**. Numbers of presumed functional synapses (identified as above) per 100 μm^2 of secondary and
834 tertiary dendrites of WT and YAC128 CPNs: 8.8 ± 1.1 (n=37; 2 cultures) and 6.8 ± 0.7 (n=57; 3
835 cultures), respectively. Although synapse numbers were lower in YAC128 cultures this did not
836 reach statistical significance [p=0.1039 (exact); Mann Whitney test].
837
838 **Fig 2: Spontaneous release of ER Ca^{2+} elevates YAC128 pyramidal neuron miniature EPSC**
839 **frequencies.**
840 **A and B - Hypothetical model (tested below) A.** We hypothesize, in WT cultures, spontaneous
841 Ca^{2+} release from ER stores in presynaptic cortical terminals only minimally augments action
842 potential-independent (mini) glutamate release. **B.** Conversely, in YAC128 cultures, we
843 hypothesize spontaneous Ca^{2+} release from presynaptic ER stores is increased, and that this
844 elevates Ca^{2+}-dependent, mini glutamate release.
845 **C – H:** Voltage clamp recordings were made at -70 mV from DIV-18 cultured WT (**C – E**) and
846 YAC128 CPNs (**F – H**) in the presence of TTX (500 nM) and PTX (50 μM), under control
847 conditions and during subsequent local ryanodine (5 μM) application. Note that in the

848 representative traces from the WT CPN (**C**), ryanodine (5 μM) substantially increased the mEPSC
849 frequency, whereas the drug had little effect on the mEPSC frequency in the representative
850 YAC128 CPN (**F**). Quantifying the population data revealed that ryanodine (5 μM) significantly
851 increased the mean mEPSC frequency in WT cultured CPNs (**D**) from 6.7 ± 1.2 Hz to 11.9 ± 2.4
852 Hz, [t(12)=2.50; p=0.0280; n=13; 8 cultures; Student's paired-t test]. Ryanodine (5 μM) did not
853 significantly affect the mean WT CPN mEPSC amplitude (**E**) (control: 21.0 ± 3.2 pA, ryanodine:
854 20.2 ± 2.3 pA), [t(12)=0.65; p=0.5278; n=13; 8 cultures; Student's paired-t test]. In YAC128
855 cultures, ryanodine (5 μM) did not significantly affect the mean CPN mEPSC frequency (**G**)
856 (control: 12.0 ± 1.7 Hz, ryanodine: 13.9 ± 2.0 Hz), [t(14)=1.65; p=0.1206; n=15; 4 cultures;
857 Student's paired-t test]. Ryanodine (5 μM) also did not significantly affect the mean CPN mEPSC
858 amplitude (**H**) (control: 20.5 ± 4.4 pA, ryanodine: 19.6 ± 3.4 pA), [t(14)=0.71; p=0.4904; n=15; 4
859 cultures; Student's paired-t test].
860 **I.** Voltage clamp recordings from representative WT (top) and YAC128 (bottom) CPNs at -70 mV
861 in the presence of TTX (500 nM) and PTX (50 μM) (as before), with the addition of CPA (30 μM)
862 and in the absence of extracellular Ca^{2+}. Note in all such recording, CPNs were incubated in this
863 CPA-containing, 0 mM Ca^{2+} ECSF for a minimum of 10 min.
864 **J.** In CPA (30 μM) and in the absence of extracellular Ca^{2+}, mEPSCs were significantly less
865 frequent in YAC128 CPNs [3.3 ± 0.6 Hz (n=14; 4 cultures)] compared WT CPNs [8.4 ± 1.5 Hz
866 (n=17; 5 cultures)] under like conditions [t(29)=2.952; p=0.0062; Student's unpaired-t test].
867 **K.** In CPA (30 μM) and in the absence of extracellular Ca^{2+}, YAC128 CPNs showed a trend
868 towards a lower mean mEPSC amplitude than in WT (WT: 26.7 ± 5.2 pA, YAC128: 16.1 ± 3.3

869 pA), but this did not reach statistical significance [t(27)=1.706; p=0.0995; Student's unpaired-t
870 test].
871
872 **Supplemental Fig 2: Releasing ER Ca^{2+} with caffeine increases the CPN mEPSC frequency**
873 **in WT, but not YAC128, CPNs.**
874 Voltage clamp recordings were made from cultured WT and YAC128 CPNs at -70 mV in the
875 presence of TTX (500 nM) and PTX (50 μM), under control conditions and during subsequent
876 local caffeine (1 mM) application.
877 **A, D:** Representative traces from WT (A) and YAC128 (D) CPNs, under control (top traces) and
878 caffeine (bottom traces) conditions. In this CPN, caffeine (1 mM) substantially increased the
879 mEPSC frequency.
880 **B.** Caffeine (1 mM) significantly increased the mean mEPSC frequency in WT cultured CPNs
881 from 12.3 ± 2.5 Hz to 22.8 ± 8.0 Hz, [p=0.0076 (exact); n=16; 8 cultures; Wilcoxon matched-pairs
882 signed rank test].
883 **C.** Caffeine (1 mM) did not significantly affect the mean WT CPN mEPSC amplitude (control:
884 13.7 ± 1.9 pA, caffeine: 17.2 ± 3.4 pA), [p=0.8603 (exact); n=16; 8 cultures; Wilcoxon matched-
885 pairs signed rank test].
886 **E.** In YAC128 CPNs, caffeine (1 mM) did not significantly affect the mean CPN mEPSC
887 frequency (control: 12.0 ± 2.1 Hz, caffeine: 11.5 ± 1.9 Hz), [t(12)=0.4808; p=0.6393; n=13; 5
888 cultures; Student's paired-t test].
889 **F.** In YAC128 CPNs, caffeine (1 mM) also did not significantly affect the mean CPN mEPSC
890 amplitude (control: 14.5 ± 1.4 pA, caffeine: 14.1 ± 1.2 pA), [t(12)=0.8086; p=0.4345; n=13; 5
891 cultures; Student's paired-t test].

892 **G.** Percent change in mEPSC frequency mediated by Caffeine (1 mM) application to WT and
893 YAC128 CPNs (calculated from the responses in panels **B** and **E**). Caffeine (1 mM) elicited a
894 significantly greater increase in the mEPSC frequency in WT, compared to YAC128, CPNs [WT:
895 99.2 ± 34.1 % (n=16; 8 cultures), YAC128: 1.2 ± 7.6 % (n=13; 5 cultures)], [p=0.0025 (exact);
896 Mann Whitney test].
897
898 **Fig 3: Axonal Ca^{2+} waves are more frequent in YAC128 Cortical Cultures.**
899 **A.** Portion of a YAC128 rat synaptophysin-tagged GCaMP6-M (rSyph-GCaMP6m)-expressing
900 axon during a spontaneous Ca^{2+} wave in the presence of ECF containing TTX (500 nM). Images
901 reflect raw GCaMP fluorescence values (arbitrary units) and comprise 15 s of a 4 min video. For
902 illustrative purposes, images were binned temporally from the original 10 Hz movie, such that
903 each 2 s frame reflects the average fluorescence of 20 successively acquired frames.
904 **B.** Time course of DF/F (change in fluorescence over basal fluorescence) values extracted from 3
905 of the YAC128 rSyph-GCaMP6m-expressing axonal boutons (shown in panel **A** with color-coded
906 arrows, panel labelled 15s). Signals were spatially averaged across elliptical regions of interest
907 (ROI)s encompassing the indicated boutons and represent the entire 4 min imaging session. Note
908 the multi-second delay in the propagation of signals between boutons and the long time course of
909 individual events.
910 **C.** Representative 3 min DF/F time course from a WT rSyph-GCaMP6m-expressing axonal bouton
911 in TTX (500 nM) (top). Note the substantially longer duration of this event compared to
912 representative events recorded without TTX from a separate WT rSyph-GCaMP6m-expressing
913 bouton (bottom).

914 **D.** Average half amplitude width of spontaneous Ca^{2+} events occurring in rSyph-GCaMP6m-
915 expressing boutons in WT and YAC128 cortical cultures in the presence and absence of TTX (500
916 nM). Select comparisons were made with the Mann Whitney test because event widths in all
917 groups failed the D'Agostino-Pearson omibus normality test. WT events were significantly longer
918 with TTX [8.60 ± 0.92 s (n=164 events; 85 boutons; 4 cultures)] than without [1.06 ± 0.97 s
919 (n=3725 events; 175 boutons; 4 cultures)] [p<0.0001 (approximate); Mann Whitney test].
920 Likewise, YAC128 half widths were significantly longer with TTX [6.23 ± 0.35 s (n=440 events;
921 153 boutons; 4 cultures)] than without [1.17 ± 1.46 s (n=5159 events; 422 boutons; 6 cultures)]
922 [p<0.0001 (approximate); Mann Whitney test].
923 **E.** Numbers of detected spontaneous axonal events (as in Panels **A** and **B**) during 3 min recordings
924 of 63 x objective (178.6 μm x 113.1 μm) fields imaged in the presence of TTX (500 nM). Action
925 potential-independent events were significantly more frequent in YAC128 cortical cultures [115.9
926 ± 28.1 events/3 min (n=15 fields; 4 cultures)], compared to WT [36.3 ± 5.5 events/3 min (n=12
927 fields; 4 cultures)], [p=0.0016 (exact); Mann Whitney test].
928 **F.** Average peak DF/F amplitudes of all the spontaneous, action potential-independent axonal Ca^{2+}
929 events imaged in a given 63 x objective field over 3 min from WT and YAC128 cortical cultures.
930 Average event amplitudes were not significantly different between WT [0.240 ± 0.046 DF/F (n=10
931 fields; 4 cultures)] and YAC128 cultures [0.216 ± 0.027 DF/F (n=12 fields; 4 cultures)],
932 [t(20)=0.465; p=0.647; Student's unpaired-t test].
933
934 **Fig 4: Boutons spontaneously active in TTX show relatively elevated cytosolic Ca^{2+} in both**
935 **genotypes. Resting cytosolic Ca^{2+} concentrations are higher in the overall YAC128 bouton**
936 **population.**

937 **A.** DF/F time courses from two rSyph-GCaMP6m-expressing axonal boutons from a
938 representative YAC128 culture in the presence of TTX (500 nM). The first bouton (top trace) is
939 inactive during the 3 min imaging session, while the second bouton (bottom trace) shows a clear
940 spontaneous event (black arrow). Subsequent application of the Ca^{2+} ionophore ionomycin (10
941 μM) elicits a smaller Ca^{2+} response in the spontaneously active bouton, suggesting a higher basal
942 cytosolic Ca^{2+} concentration (pre-ionomycin) in the active bouton.
943 **B,C:** Ionomycin responses of rSyph-GCaMP6m-expressing boutons in the presence of TTX
944 following a 3 min imaging session in WT (**B**) and YAC128 (**C**) cultures. Boutons were classified
945 as active or inactive based on the presence, or lack thereof, of at least one spontaneous Ca^{2+} event
946 during the initial 3 minute recording. Ionomycin responses were significantly larger in the
947 population of inactive boutons [WT: 0.633 ± 0.072 DF/F (n=67 boutons); YAC128: 0.410 ± 0.040
948 DF/F (n=51 boutons)], vs active boutons [WT: 0.191 ± 0.026 DF/F (n=41 boutons; 4 cultures),
949 $p<0.0001$ (exact) by Mann Whitney test; YAC128: 0.149 ± 0.016 DF/F (n=46 boutons), $p<0.0001$
950 (exact) by Mann Whitney test]. 4 cultures for WT and 4 cultures for YAC128.
951 **D, E:** Responses of rSyph-GCaMP6m-expressing axons from a representative WT (**D**) and
952 YAC128 (**E**) cortical culture to ionomycin (10 μM). Images are from a 4 min imaging session,
953 with ionomycin application at 3 min and reflect raw GCaMP fluorescence values (arbitrary units)
954 (as above). To minimize impacts of photobleaching, the top (before) image is the frame
955 immediately prior ionomycin. The bottom image is a maximum projection of all frames acquired
956 30s prior and following ionomycin treatment and reflect each pixel's maximum ionomycin
957 response. The visible grey-value dynamic range is the same in panels **D** and **E**, (150 increments of
958 the total unprocessed 14 bit-depth), however the 0 value in **E** has been adjusted so that brightness

959 of the before image is comparable to that of its WT counterpart in **D**; this is so the reader can better
960 appreciate the YAC128 culture's smaller relative change in fluorescence.
961 **F.** Ionomycin responses of the all WT and YAC128 rSyph-GCaMP6m-expressing axons
962 automatically detected with the aQua software suite (see methods for reference). The WT bouton
963 population showed a significantly greater ionomycin-mediated change in fluorescence [0.272 ±
964 0.006 DF/F (n=1681 boutons; 4 cultures)] compared to the YAC128 population [0.190 ± 0.002
965 DF/F (n=1462 boutons; 4 cultures)], [p<0.0001 (exact); Mann Whitney test].
966
967 **Fig 5: Caffeine increases the frequency of spontaneous Ca^{2+} events and the resting Ca^{2+}**
968 **concentration in WT, but not YAC128, cortical axonal boutons.**
969 **A, B:** Numbers of detected spontaneous rSyph-GCaMP6m axonal events in the presence TTX
970 (500 nM) during 3 min recordings of 63 x objective fields of WT (**A**) and YAC128 (**B**) cortical
971 cultures (as above). The control group consists of the same culture fields shown in **Figure 6: E**,
972 and is compared to separate WT (**A**) or YAC128 (**B**) culture fields imaged in the presence of
973 caffeine (1 mM) under otherwise like conditions. WT axons showed significantly more action
974 potential-independent events in the presence of caffeine, than in its absence [203.8 ± 55.2 events/3
975 min (n=10 fields; 5 cultures)] vs [36.3 ± 5.5 events/3 min (n=12 fields; 4 cultures)] respectively
976 [t(20)=3.316; p=0.0034; Student's unpaired-t test]. Numbers of detected YAC128 axonal events
977 were not significantly different in the presence or absence of caffeine [115.1 ± 28.21 events/3 min
978 (n=15 fields; 4 cultures)] vs [150.0 ± 28.55 events/3 min (n=8 fields; 4 cultures)] respectively
979 [p=0.2188 (exact); Mann Whitney test].
980 **C.** DF/F time courses from representative WT (top) and YAC128 (bottom) rSyph-GCaMP6m-
981 expressing axonal boutons in the presence of TTX (500 nM) before and immediately following

982 application of caffeine (1 mM). For this illustration, boutons were selected which did not show
983 spontaneous events. Rather, note the gradual sustained increase in rSyph-GCaMP6m fluorescence,
984 which is of larger magnitude in the WT bouton.
985 **D.** Caffeine responses of WT and YAC128 rSyph-GCaMP6m-expressing boutons in the presence
986 of TTX as illustrated in panel **C.** Boutons showing spontaneous events **(as in Figure 6)** were
987 excluded as the long time course of such events complicated quantification of steady-state
988 increases in DF/F. Caffeine application elicited a significantly greater increase in rSyph-
989 GCaMP6m fluorescence in WT boutons [0.342 ± 0.030 DF/F (n=87 boutons)] compared to
990 YAC128 [0.229 ± 0.039 DF/F (n=54 boutons)] [p=0.0004 (exact); Mann Whitney test]. For A, B
991 and D: 5 cultures for WT and 5 cultures for YAC128.
992
993 **Fig 6: In the absence of TTX, presynaptic calcium events are more frequent in WT,**
994 **compared to YAC128, cultures.**
995 **A, B:** DF/F time course from representative WT rSyph-GCaMP6m-expressing axonal boutons in
996 the absence of TTX, under control conditions (A) and in presences of 5 μM ryanodine (B). Note
997 these are not the same boutons, as experiments illustrated in this figure were not paired.
998 **C, D:** DF/F time course from two different representative YAC128 rSyph-GCaMP6m-expressing
999 axonal boutons in the absence of TTX, one under control conditions (C) and the other in the
1000 presence of 5 μM ryanodine. (D)
1001 **E:** Mean Ca^{2+} event frequencies of rSyph-GCaMP6m-expressing boutons in the absence of TTX
1002 in WT and YAC128 cortical cultures in the presence and absence of ryanodine (5 μM). Select
1003 comparisons were made with the Mann Whitney test because event widths in all groups failed the
1004 D'Agostino-Pearson omibus normality test. Events were significantly more frequent in WT

1005 boutons [0.1424 ± 0.0061 Hz (n=272 boutons; 5 cultures)] than in YAC128 boutons [0.0761 ±
1006 0.0044 Hz (n=423 boutons; 6 cultures)] [p<0.0001 (approximate); Mann Whitney test]. Events
1007 were significantly less frequent in WT boutons with ryanodine (5 μM) [0.1179 ± 0.0033 Hz (n=120
1008 boutons, 3 cultures)] than without (above) [p=0.0038 (approximate); Mann Whitney test].
1009 Conversely, event frequencies were significantly more frequent in YAC128 boutons with
1010 ryanodine (5 μM) [0.0886 ± 0.0044 Hz (n=189 boutons, 4 cultures)] than without (above)
1011 [p=0.0003 (approximate); Mann Whitney test].
1012 **F, G:** DF/F time course from two representative rSyph-GCaMP6m-expressing axonal boutons
1013 from the same WT culture field in the absence of TTX. Bouton (F) shows only faster events (lasting
1014 < 6 s), while in bouton (G) a clear slow event (lasting >6 s) is present. Note the substantially lower
1015 overall event frequency in (G).
1016 **H, I:** Ca^{2+} event frequencies of WT (H) and YAC128 (I) rSyph-GCaMP6m-expressing boutons
1017 (as above), grouped based on the presence or absence of one or more slow events (> 6 s at half
1018 peak amp). (H): 23/292 (7.9 %) WT boutons showed at least on such slow event with an overall
1019 mean bouton frequency of 0.107 ± 0.016 Hz (n=23), significantly lower than WT boutons lacking
1020 slower events [0.143 ± 0.006 Hz (n=269)] [p=0.0058 (exact); Mann Whitney test] (n=292 boutons,
1021 5 cultures). (I) 44/423 (10.4 %) YAC128 boutons showed at least one such slow event with an
1022 overall mean bouton frequency of 0.052 ± 0.005 Hz (n=44), significantly lower than YAC128
1023 boutons lacking slower events [0.076 ± 0.004 Hz (n=379)] [p=0.0058 (exact); Mann Whitney test]
1024 (n=423 boutons, 6 cultures).
1025
1026 **Fig 7: Ryanodine reduces evoked striatal iGluSnR responses in WT, but not YAC128, brain**
1027 **slices.**

1028 **A.** Image of raw iGluSnFR fluorescence from a representative WT mouse brain slice with viral-
1029 mediated expression of iGluSnFR in its dorsal striatum. Note the square ROI over which evoked
1030 spatially averaged DF/F signals were measured, and the tungsten monopolar stimulating electrode
1031 placed in the corpus callosum.
1032 **B.** A DF/F image montage from the WT brain slice (shown in A), illustrating a striatum iGluSnFR
1033 response evoked by electrically stimulating cortical axons in the adjacent corpus callosum.
1034 **C.** Striatum evoked DF/F iGluSnFR responses from a representative WT (top) and YAC128
1035 (bottom) brain slice before and in the presence of ryanodine (5 μM). Ryanodine elicits a substantial
1036 reduction in the peak WT, but not YAC128, iGluSnFR response.
1037 **D.** Peak evoked striatum iGluSnFR responses from WT and YAC128 slices before and during
1038 treatment of slices with ryanodine (5 μM). Responses were measured repeatedly at 3 min intervals
1039 and were normalized to the average of each slice's 3 baseline (before drug) measurements.
1040 Ryanodine application decreased the amplitude of the evoked iGluSnFR response in WT (n=9
1041 slices; 9 mice), but not YAC128 (n=8 slices; 8 mice). The effect of ryanodine on WT slices was
1042 significantly different than in YAC128 slices, based on a significant time-genotype interaction
1043 (p=0.0094, repeated measure (time) two way ANOVA).
1044
1045
1046
1047

References:

A novel gene containing a trinucleotide repeat that is expanded and unstable on Huntington“s disease chromosomes. The Huntington”s Disease Collaborative Research Group. (1993). A novel gene containing a trinucleotide repeat that is expanded and unstable on Huntington“s disease chromosomes. The Huntington”s Disease Collaborative Research Group. *Cell*, *72*(6), 971–983.

Atasoy, D., Ertunc, M., Moulder, K. L., Blackwell, J., Chung, C., Su, J., & Kavalali, E. T. (2008). Spontaneous and evoked glutamate release activates two populations of NMDA receptors with limited overlap. *The Journal of Neuroscience : the Official Journal of the Society for Neuroscience*, *28*(40), 10151–10166. http://doi.org/10.1523/JNEUROSCI.2432-08.2008

Bachoud-Lévi, A.-C., Ferreira, J., Massart, R., Youssov, K., Rosser, A., Busse, M., et al. (2019). International Guidelines for the Treatment of Huntington's Disease. *Frontiers in Neurology*, *10*, 710. http://doi.org/10.3389/fneur.2019.00710

Beal, M. F., Kowall, N. W., Ellison, D. W., Mazurek, M. F., Swartz, K. J., & Martin, J. B. (1986). Replication of the neurochemical characteristics of Huntington's disease by quinolinic acid. *Nature*, *321*(6066), 168–171. http://doi.org/10.1038/321168a0

Beaulieu-Laroche, L., & Harnett, M. T. (2018). Dendritic Spines Prevent Synaptic Voltage Clamp. *Neuron*, *97*(1), 75–82.e3. http://doi.org/10.1016/j.neuron.2017.11.016

Botelho, E. P., Wang, E., Chen, J. Y., Holley, S., Andre, V., Cepeda, C., & Levine, M. S. (2014). Differential Synaptic and Extrasynaptic Glutamate-Receptor Alterations in Striatal Medium-Sized Spiny Neurons of Aged YAC128 Huntington's Disease Mice. *PLoS Currents*, *6*. http://doi.org/10.1371/currents.hd.34957c4f8bd7cb1f5ec47381dfc811c3

Budde, T., Meuth, S., & Pape, H.-C. (2002). Calcium-dependent inactivation of neuronal calcium channels. *Nature Reviews. Neuroscience*, *3*(11), 873–883. http://doi.org/10.1038/nrn959

Buren, C., Parsons, M. P., Smith-Dijak, A., & Raymond, L. A. (2016). Impaired development of cortico-striatal synaptic connectivity in a cell culture model of Huntington's disease. *Neurobiology of Disease*, *87*, 80–90. http://doi.org/10.1016/j.nbd.2015.12.009

Cens, T., Rousset, M., Leyris, J.-P., Fesquet, P., & Charnet, P. (2006). Voltage- and calcium-dependent inactivation in high voltage-gated Ca(2+) channels. *Progress in Biophysics and Molecular Biology*, *90*(1-3), 104–117. http://doi.org/10.1016/j.pbiomolbio.2005.05.013

Cepeda, C., Hurst, R. S., Calvert, C. R., Hernández-Echeagaray, E., Nguyen, O. K., Jocoy, E., et al. (2003). Transient and progressive electrophysiological alterations in the corticostriatal pathway in a mouse model of Huntington's disease. *The Journal of Neuroscience : the Official Journal of the Society for Neuroscience*, *23*(3), 961–969.

Chen, T.-W., Wardill, T. J., Sun, Y., Pulver, S. R., Renninger, S. L., Baohan, A., et al. (2013). Ultrasensitive fluorescent proteins for imaging neuronal activity. *Nature*, *499*(7458), 295–300. http://doi.org/10.1038/nature12354

de Juan-Sanz, J., Holt, G. T., Schreiter, E. R., de Juan, F., Kim, D. S., & Ryan, T. A. (2017). Axonal Endoplasmic Reticulum Ca 2+ Content Controls Release Probability in CNS Nerve Terminals. *Neuron*, *93*(4), 867–881.e6. http://doi.org/10.1016/j.neuron.2017.01.010

Dunwiddie, T. V., & Masino, S. A. (2001). The role and regulation of adenosine in the central nervous system. *Annual Review of Neuroscience*, *24*(1), 31–55. http://doi.org/10.1146/annurev.neuro.24.1.31

Emptage, N. J., Reid, C. A., & Fine, A. (2001). Calcium Stores in Hippocampal Synaptic Boutons Mediate Short-Term Plasticity, Store-Operated Ca2+ Entry, and Spontaneous Transmitter Release. *Neuron*, *29*(1), 197–208. http://doi.org/10.1016/S0896-6273(01)00190-8

Espinosa, F., & Kavalali, E. T. (2009). NMDA Receptor Activation by Spontaneous Glutamatergic Neurotransmission. *Journal of Neurophysiology*, *101*(5), 2290–2296. http://doi.org/10.1152/jn.90754.2008

Fan, M. M. Y., Fernandes, H. B., Zhang, L. Y. J., Hayden, M. R., & Raymond, L. A. (2007). Altered NMDA receptor trafficking in a yeast artificial chromosome transgenic mouse model of Huntington's disease. *The Journal of Neuroscience : the Official Journal of the Society for Neuroscience*, *27*(14), 3768–3779. http://doi.org/10.1523/JNEUROSCI.4356-06.2007

Fishbein, I., & Segal, M. (2007). Miniature synaptic currents become neurotoxic to chronically silenced neurons. *Cerebral Cortex (New York, N.Y. : 1991)*, *17*(6), 1292–1306. http://doi.org/10.1093/cercor/bhl037

Frank, C. A., Kennedy, M. J., Goold, C. P., Marek, K. W., & Davis, G. W. (2006). Mechanisms underlying the rapid induction and sustained expression of synaptic homeostasis. *Neuron*, *52*(4), 663–677. http://doi.org/10.1016/j.neuron.2006.09.029

Fredj, N. B., & Burrone, J. (2009). A resting pool of vesicles is responsible for spontaneous vesicle fusion at the synapse. *Nature Neuroscience*, *12*(6), 751–758. http://doi.org/10.1038/nn.2317

Graveland, G. A., Williams, R. S., & DiFiglia, M. (1985). Evidence for degenerative and regenerative changes in neostriatal spiny neurons in Huntington's disease. *Science (New York, N.Y.)*, *227*(4688), 770–773.

Gross, G. G., Junge, J. A., Mora, R. J., Kwon, H.-B., Olson, C. A., Takahashi, T. T., et al. (2013). Recombinant probes for visualizing endogenous synaptic proteins in living neurons. *Neuron*, *78*(6), 971–985. http://doi.org/10.1016/j.neuron.2013.04.017

Hantraye, P., Riche, D., Maziere, M., & Isacson, O. (1990). A primate model of Huntington's disease: behavioral and anatomical studies of unilateral excitotoxic lesions of the caudate-putamen in the baboon. *Experimental Neurology*, *108*(2), 91–104.

Joshi, P. R., Wu, N.-P., André, V. M., Cummings, D. M., Cepeda, C., Joyce, J. A., et al. (2009). Age-dependent alterations of corticostriatal activity in the YAC128 mouse model of Huntington disease. *The Journal of Neuroscience : the Official Journal of the Society for Neuroscience*, *29*(8), 2414–2427. http://doi.org/10.1523/JNEUROSCI.5687-08.2009

Kavalali, E. T. (2015). The mechanisms and functions of spontaneous neurotransmitter release. *Nature Reviews. Neuroscience*, *16*(1), 5–16. http://doi.org/10.1038/nrn3875

Kovalenko, M., Milnerwood, A., Giordano, J., St Claire, J., Guide, J. R., Stromberg, M., et al. (2018). HttQ111/+ Huntington's Disease Knock-in Mice Exhibit Brain Region-Specific Morphological Changes and Synaptic Dysfunction. *Journal of Huntington's Disease*, *7*(1), 17–33. http://doi.org/10.3233/JHD-170282

Lindhout, F. W., Cao, Y., Kevenaar, J. T., Bodzęta, A., Stucchi, R., Boumpoutsari, M. M., et al. (2019). VAP-SCRN1 interaction regulates dynamic endoplasmic reticulum remodeling and

presynaptic function. *The EMBO Journal*, *38*(20), e101345. http://doi.org/10.15252/embj.2018101345

Llano, I., González, J., Caputo, C., Lai, F. A., Blayney, L. M., Tan, Y. P., & Marty, A. (2000). Presynaptic calcium stores underlie large-amplitude miniature IPSCs and spontaneous calcium transients. *Nature Neuroscience*, *3*(12), 1256–1265. http://doi.org/10.1038/81781

McKinney, R. A., Capogna, M., Dürr, R., Gähwiler, B. H., & Thompson, S. M. (1999). Miniature synaptic events maintain dendritic spines via AMPA receptor activation. *Nature Neuroscience*, *2*(1), 44–49. http://doi.org/10.1038/4548

Meissner, G. (2017). The structural basis of ryanodine receptor ion channel function. *The Journal of General Physiology*, *149*(12), 1065–1089. http://doi.org/10.1085/jgp.201711878

Miller, B. R., Dorner, J. L., Shou, M., Sari, Y., Barton, S. J., Sengelaub, D. R., et al. (2008). Up-regulation of GLT1 expression increases glutamate uptake and attenuates the Huntington's disease phenotype in the R6/2 mouse. *Neuroscience*, *153*(1), 329–337. http://doi.org/10.1016/j.neuroscience.2008.02.004

Milnerwood, A. J., Gladding, C. M., Pouladi, M. A., Kaufman, A. M., Hines, R. M., Boyd, J. D., et al. (2010). Early Increase in Extrasynaptic NMDA Receptor Signaling and Expression Contributes to Phenotype Onset in Huntington's Disease Mice. *Neuron*, *65*(2), 178–190. http://doi.org/10.1016/j.neuron.2010.01.008

Milnerwood, A. J., Kaufman, A. M., Sepers, M. D., Gladding, C. M., Zhang, L., Wang, L., et al. (2012). Mitigation of augmented extrasynaptic NMDAR signaling and apoptosis in cortico-striatal co-cultures from Huntington's disease mice. *Neurobiology of Disease*, *48*(1), 40–51. http://doi.org/10.1016/j.nbd.2012.05.013

Morton, A. J., & Edwardson, J. M. (2001). Progressive depletion of complexin II in a transgenic mouse model of Huntington's disease. *Journal of Neurochemistry*, *76*(1), 166–172. http://doi.org/10.1046/j.1471-4159.2001.00059.x

Morton, A. J., Faull, R. L., & Edwardson, J. M. (2001). Abnormalities in the synaptic vesicle fusion machinery in Huntington's disease. *Brain Research Bulletin*, *56*(2), 111–117. http://doi.org/10.1016/s0361-9230(01)00611-6

Parsons, M. P., Vanni, M. P., Woodard, C. L., Kang, R., Murphy, T. H., & Raymond, L. A. (2016). Real-time imaging of glutamate clearance reveals normal striatal uptake in Huntington disease mouse models. *Nature Communications*, *7*, 11251. http://doi.org/10.1038/ncomms11251

Peled, E. S., Newman, Z. L., & Isacoff, E. Y. (2014). Evoked and spontaneous transmission favored by distinct sets of synapses. *Current Biology : CB*, *24*(5), 484–493. http://doi.org/10.1016/j.cub.2014.01.022

Plotkin, J. L., Day, M., Peterson, J. D., Xie, Z., Kress, G. J., Rafalovich, I., et al. (2014). Impaired TrkB Receptor Signaling Underlies Corticostriatal Dysfunction in Huntington's Disease. *Neuron*, *83*(1), 178–188. http://doi.org/10.1016/j.neuron.2014.05.032

Raymond, L. A., André, V. M., Cepeda, C., Gladding, C. M., Milnerwood, A. J., & Levine, M. S. (2011). Pathophysiology of Huntington's disease: time-dependent alterations in synaptic and receptor function. *Neuroscience*, *198*, 252–273. http://doi.org/10.1016/j.neuroscience.2011.08.052

Reese, A. L., & Kavalali, E. T. (2016). Single synapse evaluation of the postsynaptic NMDA receptors targeted by evoked and spontaneous neurotransmission. *eLife*, *5*, 6336. http://doi.org/10.7554/eLife.21170

Ross, W. N. (2012). Understanding calcium waves and sparks in central neurons. *Nature Reviews. Neuroscience*, *13*(3), 157–168. http://doi.org/10.1038/nrn3168

Sara, Y., Virmani, T., Deák, F., Liu, X., & Kavalali, E. T. (2005). An isolated pool of vesicles recycles at rest and drives spontaneous neurotransmission. *Neuron*, *45*(4), 563–573. http://doi.org/10.1016/j.neuron.2004.12.056

Sepers, M. D., Smith-Dijak, A., LeDue, J., Kolodziejczyk, K., Mackie, K., & Raymond, L. A. (2017). Endocannabinoid-specific impairment in synaptic plasticity in striatum of Huntington's disease mouse model. *The Journal of Neuroscience : the Official Journal of the Society for Neuroscience*, 1739–17. http://doi.org/10.1523/JNEUROSCI.1739-17.2017

Smith-Dijak, A. I., Nassrallah, W. B., Zhang, L. Y. J., Geva, M., Hayden, M. R., & Raymond, L. A. (2019). Impairment and Restoration of Homeostatic Plasticity in Cultured Cortical Neurons From a Mouse Model of Huntington Disease. *Frontiers in Cellular Neuroscience*, *13*, 209. http://doi.org/10.3389/fncel.2019.00209

Sutton, M. A., Ito, H. T., Cressy, P., Kempf, C., Woo, J. C., & Schuman, E. M. (2006). Miniature neurotransmission stabilizes synaptic function via tonic suppression of local dendritic protein synthesis. *Cell*, *125*(4), 785–799. http://doi.org/10.1016/j.cell.2006.03.040

Sutton, M. A., Taylor, A. M., Ito, H. T., Pham, A., & Schuman, E. M. (2007). Postsynaptic decoding of neural activity: eEF2 as a biochemical sensor coupling miniature synaptic transmission to local protein synthesis. *Neuron*, *55*(4), 648–661. http://doi.org/10.1016/j.neuron.2007.07.030

Suzuki, M., Nagai, Y., Wada, K., & Koike, T. (2012). Calcium leak through ryanodine receptor is involved in neuronal death induced by mutant huntingtin. *Biochemical and Biophysical Research Communications*, *429*(1-2), 18–23. http://doi.org/10.1016/j.bbrc.2012.10.107

Tang, T. S., Guo, C., Wang, H., Chen, X., & Bezprozvanny, I. (2009). Neuroprotective Effects of Inositol 1,4,5-Trisphosphate Receptor C-Terminal Fragment in a Huntington's Disease Mouse Model. *Journal of Neuroscience*, *29*(5), 1257–1266. http://doi.org/10.1523/JNEUROSCI.4411-08.2009

Tang, T.-S., Tu, H., Chan, E. Y. W., Maximov, A., Wang, Z., Wellington, C. L., et al. (2003). Huntingtin and huntingtin-associated protein 1 influence neuronal calcium signaling mediated by inositol-(1,4,5) triphosphate receptor type 1. *Neuron*, *39*(2), 227–239.

Tyebji, S., & Hannan, A. J. (2017). Synaptopathic mechanisms of neurodegeneration and dementia: Insights from Huntington's disease. *Progress in Neurobiology*, *153*, 18–45. http://doi.org/10.1016/j.pneurobio.2017.03.008

van de Vrede, Y., Fossier, P., Baux, G., Joels, M., & Chameau, P. (2007). Control of IsAHP in mouse hippocampus CA1 pyramidal neurons by RyR3-mediated calcium-induced calcium release. *Pflugers Archiv : European Journal of Physiology*, *455*(2), 297–308. http://doi.org/10.1007/s00424-007-0277-4

Vonsattel, J. P., Myers, R. H., Stevens, T. J., Ferrante, R. J., Bird, E. D., & Richardson, E. P. (1985). Neuropathological classification of Huntington's disease. *Journal of Neuropathology and Experimental Neurology*, *44*(6), 559–577.

Wang, R., & Reddy, P. H. (2017). Role of Glutamate and NMDA Receptors in Alzheimer's Disease. *Journal of Alzheimer's Disease : JAD*, *57*(4), 1041–1048. http://doi.org/10.3233/JAD-160763

Wang, Y., DelRosso, N. V., Vaidyanathan, T. V., Cahill, M. K., Reitman, M. E., Pittolo, S., et al. (2019). Accurate quantification of astrocyte and neurotransmitter fluorescence dynamics for

single-cell and population-level physiology. *Nature Neuroscience*, *22*(11), 1936–1944. http://doi.org/10.1038/s41593-019-0492-2

Xu, J., Pang, Z. P., Shin, O.-H., & Südhof, T. C. (2009). Synaptotagmin-1 functions as a Ca2+ sensor for spontaneous release. *Nature Neuroscience*, *12*(6), 759–766. http://doi.org/10.1038/nn.2320

Zeron, M. M., Hansson, O., Chen, N., Wellington, C. L., Leavitt, B. R., Brundin, P., et al. (2002). Increased Sensitivity to N-Methyl-D-Aspartate Receptor-Mediated Excitotoxicity in a Mouse Model of Huntington's Disease. *Neuron*, *33*(6), 849–860. http://doi.org/10.1016/S0896-6273(02)00615-3

Figure 1:

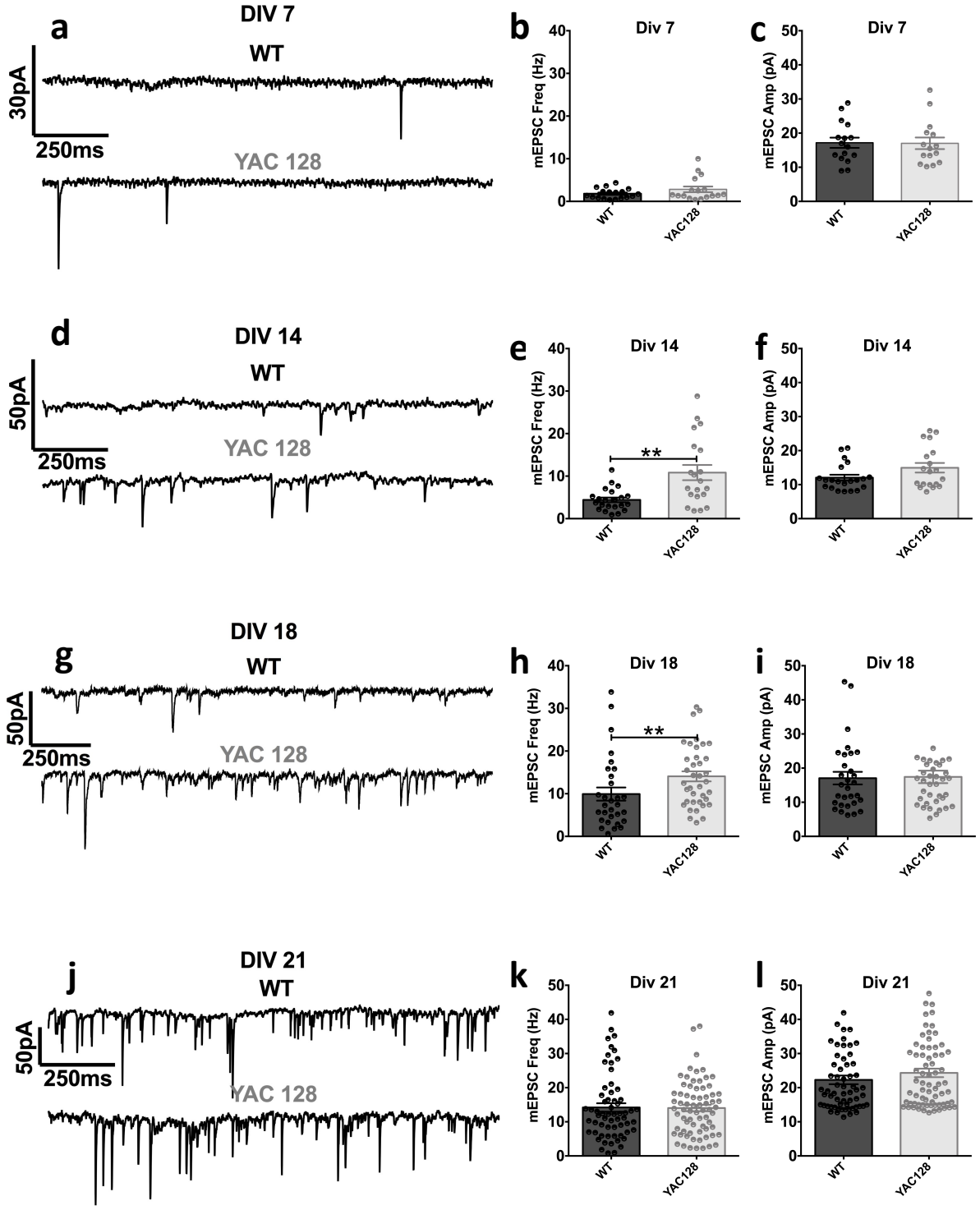
a
DIV 7
WT
30pA
250ms
YAC 128
b
Div 7
mEPSC Freq (Hz)
WT
YAC128
c
Div 7
mEPSC Amp (pA)
WT
YAC128
d
DIV 14
WT
50pA
250ms
YAC 128
e
Div 14
mEPSC Freq (Hz)
**
WT
YAC128
f
Div 14
mEPSC Amp (pA)
WT
YAC128
g
DIV 18
WT
50pA
250ms
YAC 128
h
Div 18
mEPSC Freq (Hz)
**
WT
YAC128
i
Div 18
mEPSC Amp (pA)
WT
YAC128
j
DIV 21
WT
50pA
250ms
YAC 128
k
Div 21
mEPSC Freq (Hz)
WT
YAC128
l
Div 21
mEPSC Amp (pA)
WT
YAC128

Supplemental Figure 1:

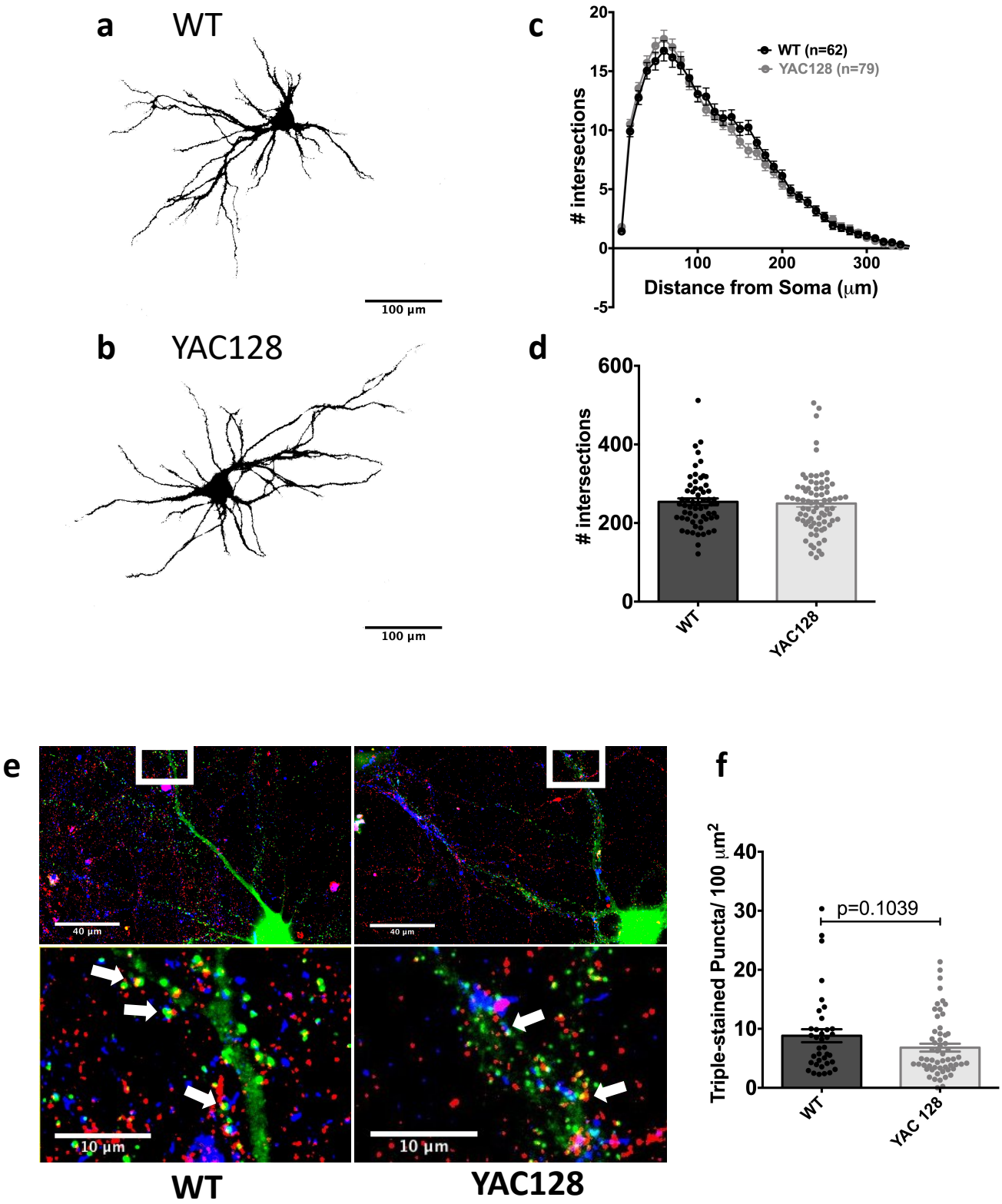

Figure 2:

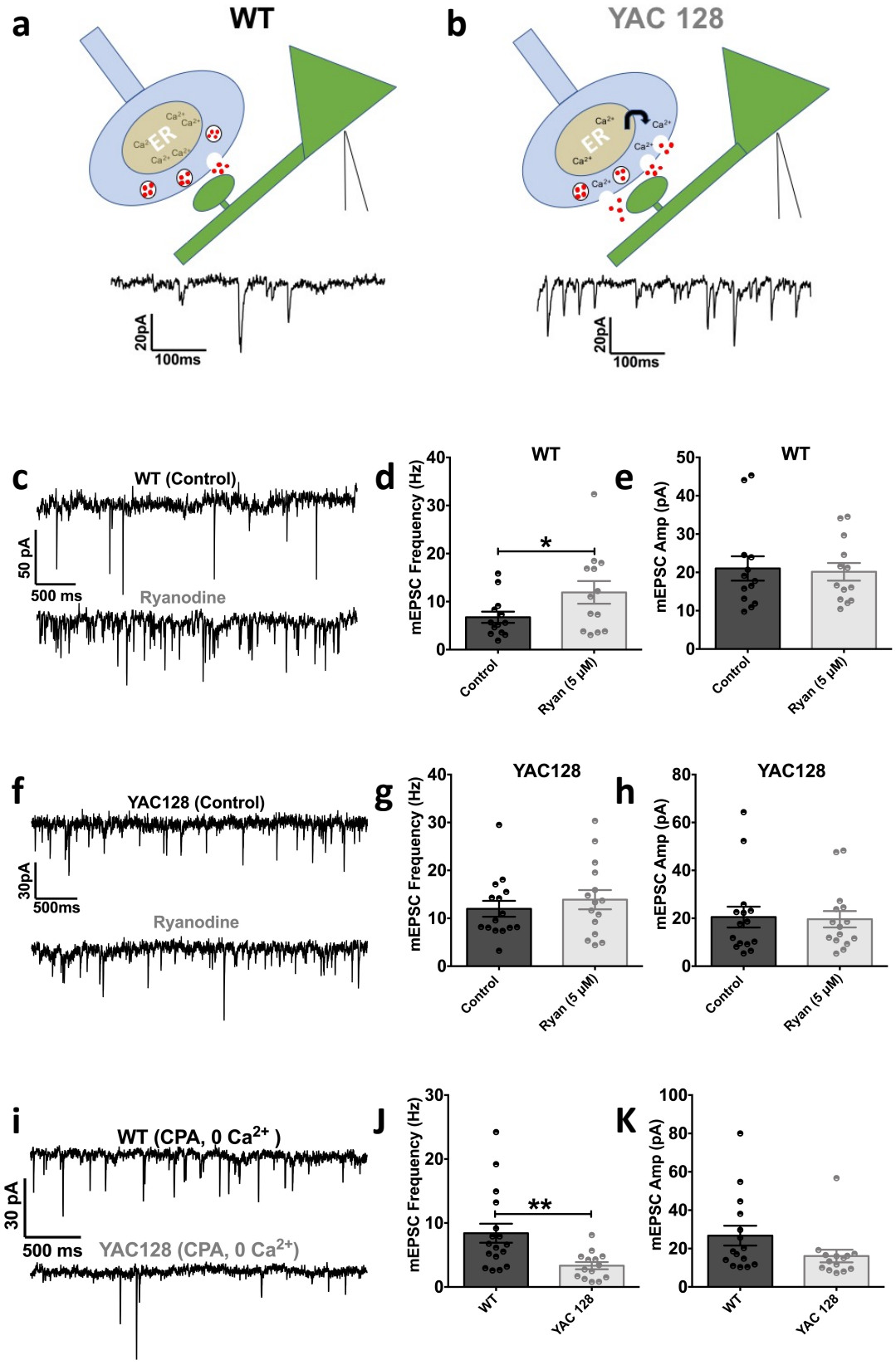
a
WT
ER
20pA
100ms
b
YAC 128
ER
20pA
100ms
c
WT (Control)
50 pA
500 ms
Ryanodine
d
WT
mEPSC Frequency (Hz)
*
Control
Ryan (5 μM)
e
WT
mEPSC Amp (pA)
Control
Ryan (5 μM)
f
YAC128 (Control)
30pA
500ms
Ryanodine
g
YAC128
mEPSC Frequency (Hz)
Control
Ryan (5 μM)
h
YAC128
mEPSC Amp (pA)
Control
Ryan (5 μM)
i
WT (CPA, 0 Ca2+)
30 pA
500 ms
YAC128 (CPA, 0 Ca2+)
J
mEPSC Frequency (Hz)
**
WT
YAC 128
K
mEPSC Amp (pA)
WT
YAC 128

Supplemental Figure 2:

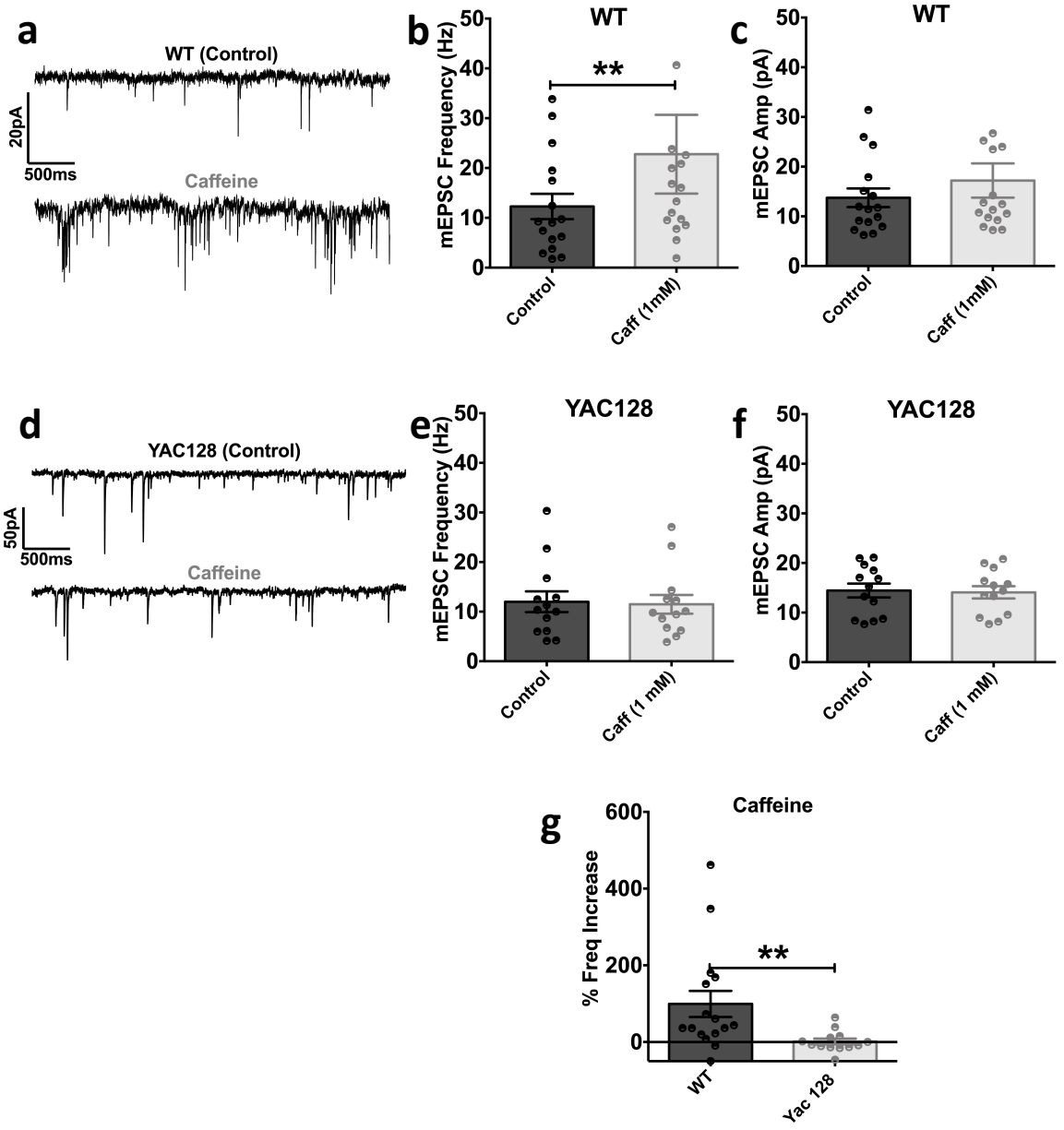

Figure 3:

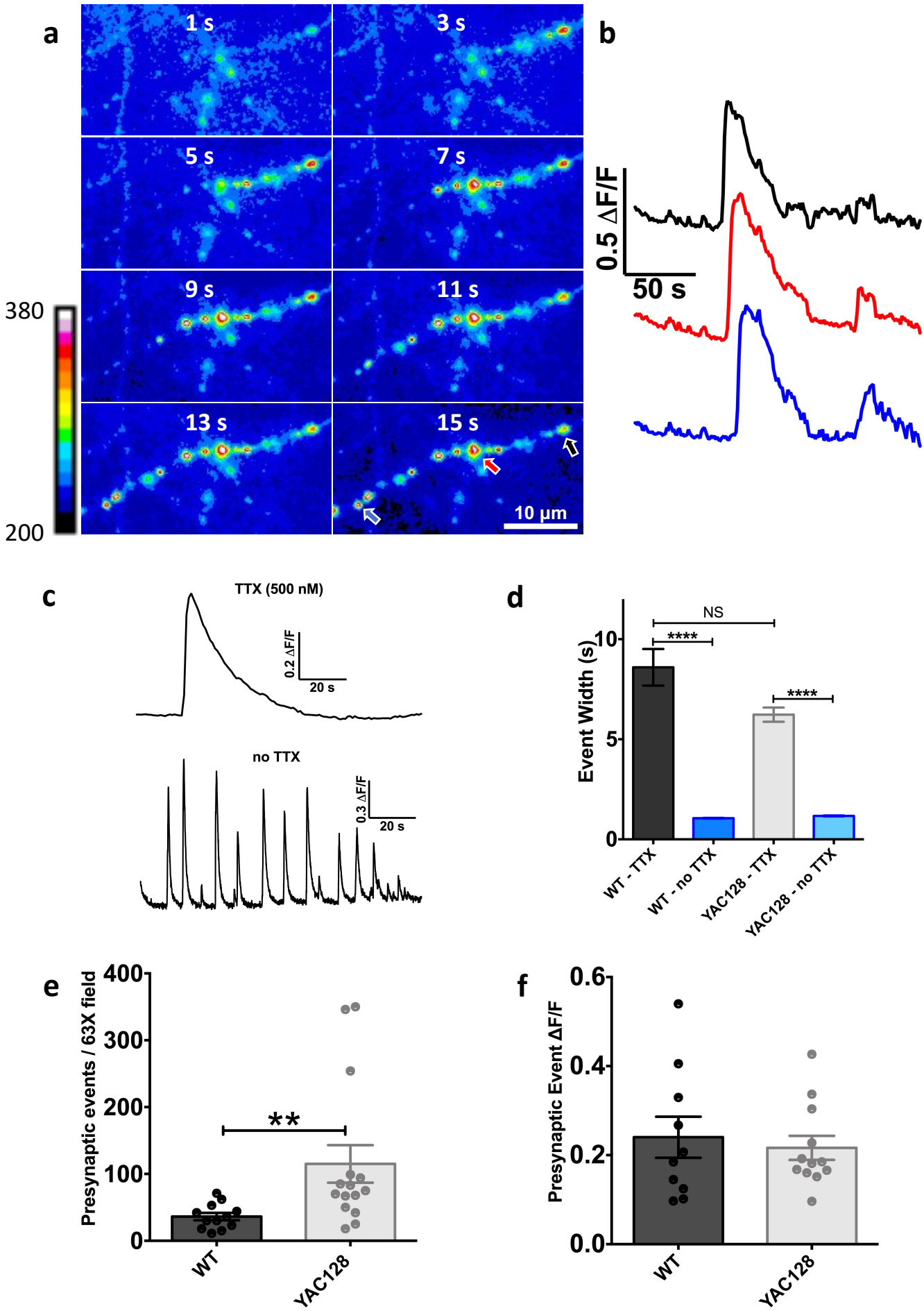
a
1 s
3 s
5 s
7 s
9 s
11 s
13 s
15 s
10 µm
380
200
b
0.5 ΔF/F
50 s
c
TTX (500 nM)
0.2 ΔF/F
20 s
no TTX
0.3 ΔF/F
20 s
d
Event Width (s)
NS
****
****
WT - TTX
WT - no TTX
YAC128 - TTX
YAC128 - no TTX
e
Presynaptic events / 63X field
**
WT
YAC128
f
Presynaptic Event ΔF/F
WT
YAC128

Figure 4:

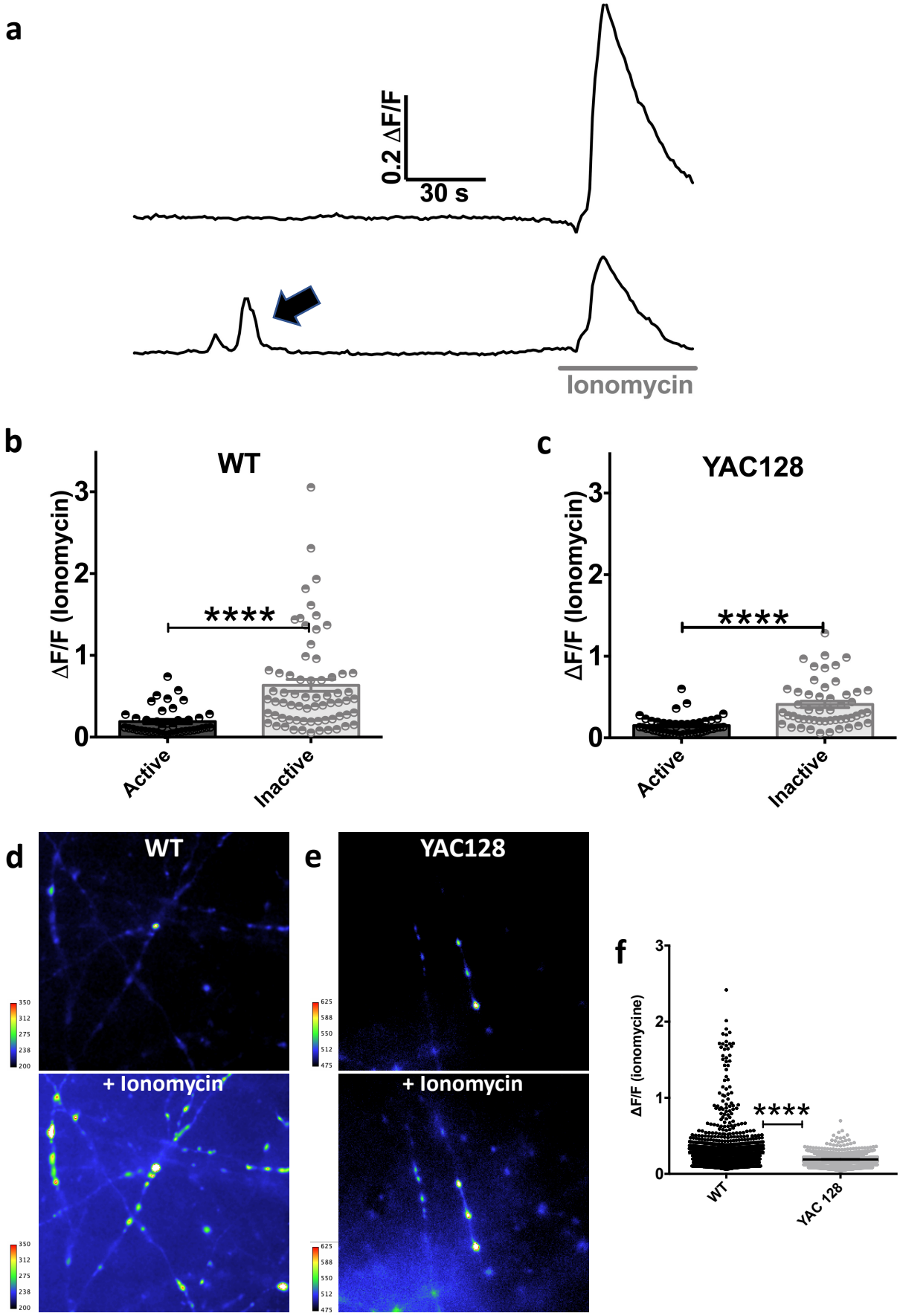
a
0.2 ΔF/F
30 s
Ionomycin
b
WT
ΔF/F (Ionomycin)
****
Active
Inactive
c
YAC128
ΔF/F (Ionomycin)
****
Active
Inactive
d
WT
+ Ionomycin
e
YAC128
+ Ionomycin
f
ΔF/F (ionomycine)
****
WT
YAC 128

Figure 5:

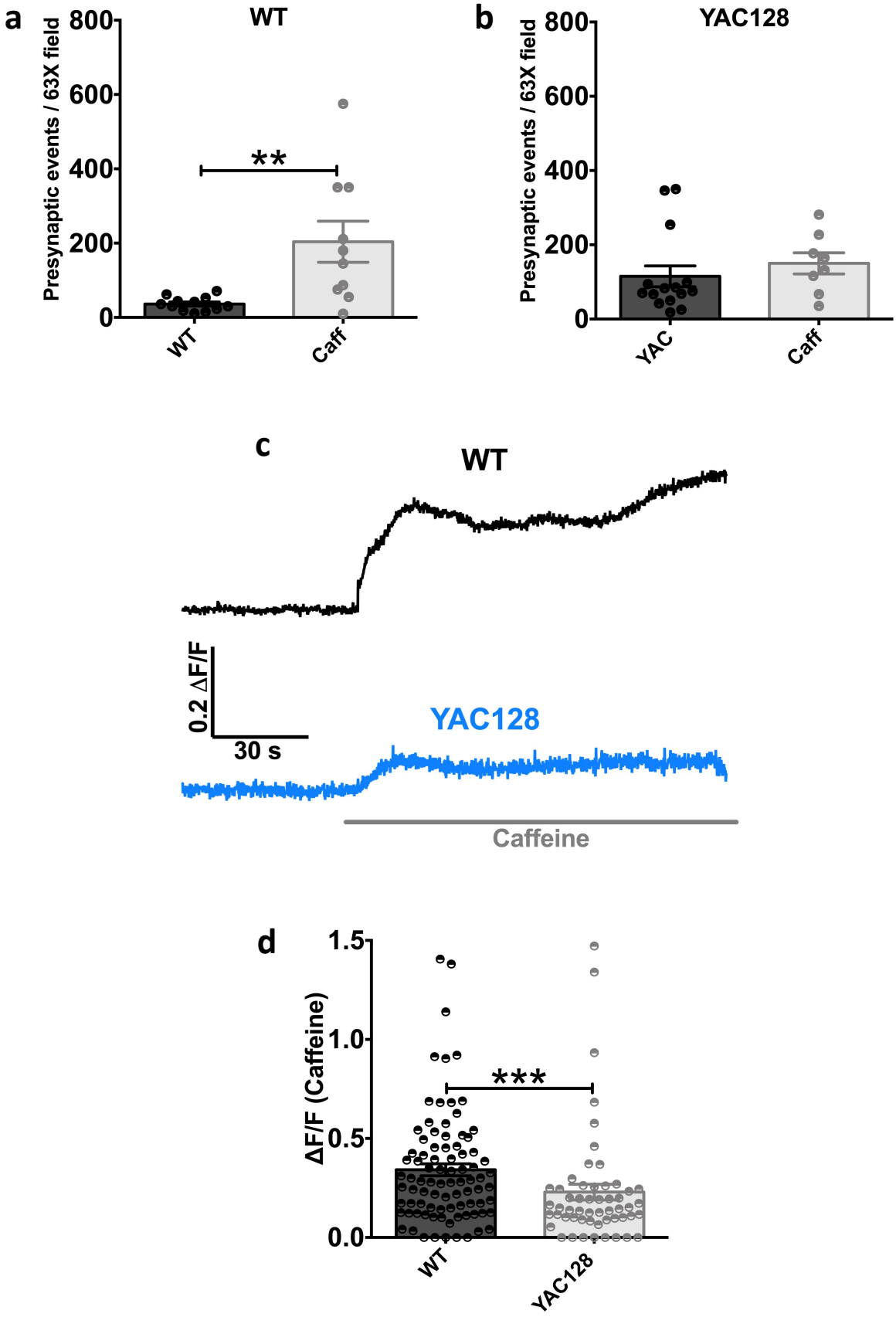
a
WT
Presynaptic events / 63X field
800
600
400
200
0
**
WT
Caff
b
YAC128
Presynaptic events / 63X field
800
600
400
200
0
YAC
Caff
c
WT
0.2 ΔF/F
30 s
YAC128
Caffeine
d
ΔF/F (Caffeine)
1.5
1.0
0.5
0.0
***
WT
YAC128

Figure 6:

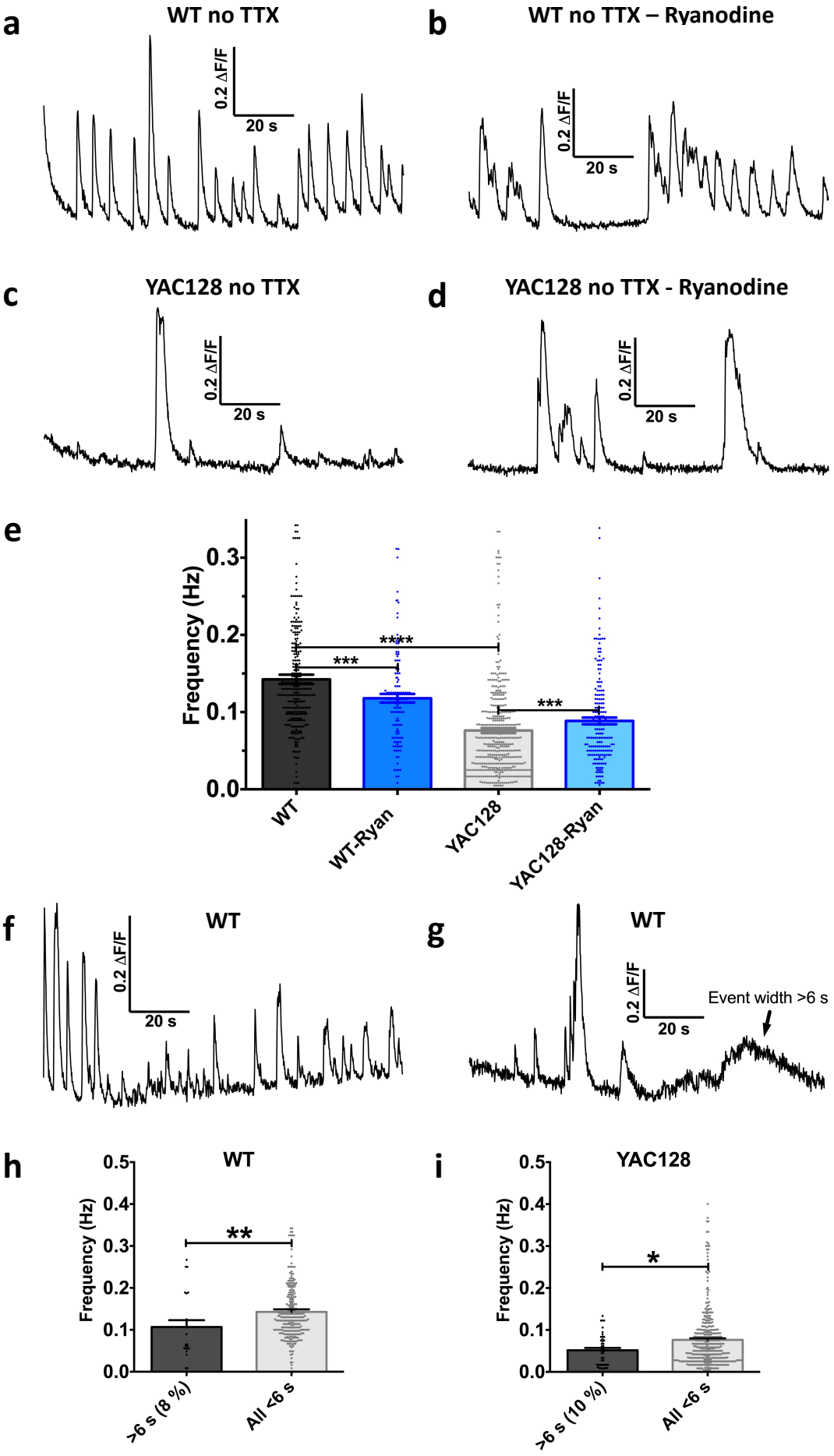
a
WT no TTX
0.2 ΔF/F
20 s
b
WT no TTX – Ryanodine
0.2 ΔF/F
20 s
c
YAC128 no TTX
0.2 ΔF/F
20 s
d
YAC128 no TTX - Ryanodine
0.2 ΔF/F
20 s
e
Frequency (Hz)
0.0
0.1
0.2
0.3
****
***
***
WT
WT-Ryan
YAC128
YAC128-Ryan
f
WT
0.2 ΔF/F
20 s
g
WT
0.2 ΔF/F
20 s
Event width >6 s
h
WT
Frequency (Hz)
0.0
0.1
0.2
0.3
0.4
0.5
**
>6 s (8 %)
All <6 s
i
YAC128
Frequency (Hz)
0.0
0.1
0.2
0.3
0.4
0.5
*
>6 s (10 %)
All <6 s

Figure 7:

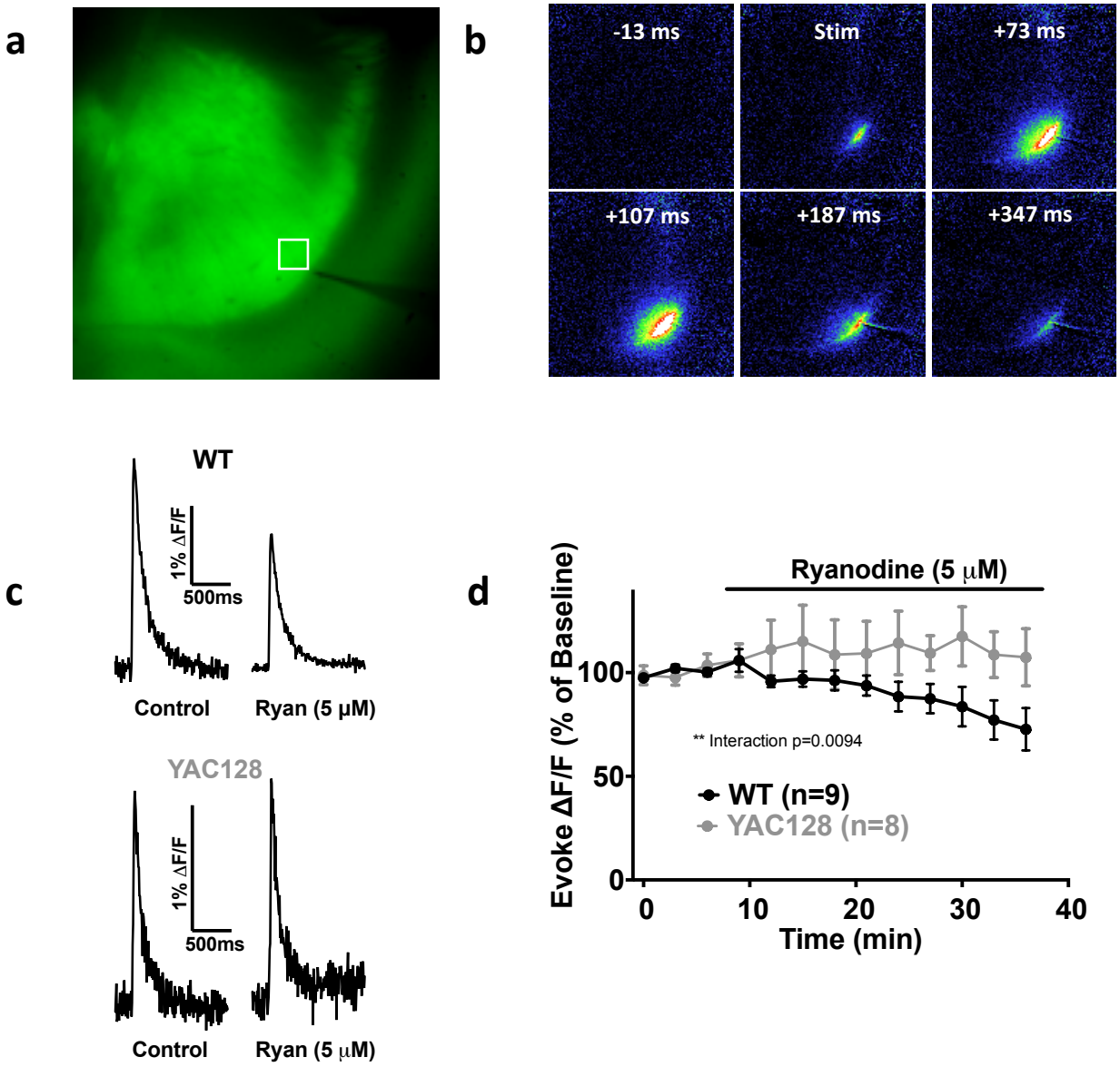
a
b
-13 ms
Stim
+73 ms
+107 ms
+187 ms
+347 ms
c
WT
1% ΔF/F
500ms
Control
Ryan (5 μM)
YAC128
1% ΔF/F
500ms
Control
Ryan (5 μM)
d
Ryanodine (5 μM)
Evoke ΔF/F (% of Baseline)
100
50
0
** Interaction p=0.0094
WT (n=9)
YAC128 (n=8)
0
10
20
30
40
Time (min)